In presenting the dissertation as a partial fulfillment of the requirements for an advanced degree from the Georgia Institute of Technology, I agree that the Library of the Institute shall make it available for inspection and circulation in accordance with its regulations governing materials of this type. I agree that permission to copy from, or to publish from, this dissertation may be granted by the professor under whose direction it was written, or, in his absence, by the Dean of the Graduate Division when such copying or publication is solely for scholarly purposes and does not involve potential financial gain. It is understood that any copying from, or publication of, this dissertation which involves potential financial gain will not be allowed without written permission.

7/25/68

STRESS CORROSION CRACKING IN ALMAR 362 MAR-AGING STAINLESS STEEL

A THESIS

Presented to

The Faculty of the Graduate Division

by

Panagiotis Kalofonos

In Partial Fulfillment

of the Requirements for the Degree

Master of Science in Metallurgy

Georgia Institute of Technology

September, 1968

STRESS CORROSION CRACKING IN ALMAR 362 MAR-AGING STAINLESS STEEL

Approved:

Chairman

Date approved by Chairman: 8/26/68

ACKNOWLEDGMENTS

The author wishes to express deep appreciation to his thesis advisor, Dr. Robert Hochman, who suggested this research project and contributed much advice and invaluable aid to this work.

Great appreciation is also extended to Dr. Edgar Starke and Dr. Bruce LeFevre for their invaluable help in obtaining electron microscopy data for this study; also to Dr. Niels Engel for his time spent in reviewing the record of this research as it was being written.

Thanks are extended to the Allegheny Ludlum Steel Corporation for its contribution of material.

Thanks are also extended to Mr. Charles R. Blackwood whose help in the machine shop led to this work.

The author's thanks and appreciation are expressed to his friends who acted as sounding boards for his ideas and gave help and advice to his research.

Finally, special thanks go to my wife, Engie, whose patience, time and help have contributed much to the completion of this work.

TABLE OF CONTENTS

TABLE OF CONTENTS (continued)

LIST OF TABLES

LIST OF FIGURES

LIST OF FIGURES (continued)

LIST OF FIGURES (continued)

SUMMARY

The object of the present investigation was to study the effect of different heat treatments and mechanical strength levels on the stress-corrosion cracking process of Almar 362 mar-aging steel.

Time to failure as a function of applied stress was determined for numerous heat treatments and for various applied external currents. Material aged at higher temperatures was found to be less susceptible to stress corrosion cracking, compared to material aged at the lower temperatures. This steel had very good resistance to cracking when aged at about 1150°F.

When the Almar 362 was austenitized, cold rolled, and then directly aged, the significant increase in tensile strength was accompanied by the highest susceptibility for hydrogen embrittlement cracking. This susceptibility diminished with decreasing strength of the steel.

Potential-time curves showed that when stress cracking occurred in a chloride solution containing acetic acid or SeO_2, an impressed anodic current of a few mA markedly increased the life of the material, whereas an impressed cathodic current decreased the time to failure. This is strong evidence to support a conclusion that in such media the Almar 362 fails by hydrogen embrittlement cracking. These corrodents were also found to play an important role in reducing the notch strength of this steel.

Metallographic and electron microscopy data indicated no difference between anodic and cathodic fractures.

CHAPTER I

INTRODUCTION

The term stress corrosion cracking (SCC) is used here to describe the process in which a crack propagates by the stress-induced corrosion of metal at the advancing tip of the crack. The stress may be either externally applied or "locked in" as from welding, heat treatment, or cold work. The corrodent need not be a bulk aqueous solution--it may be a thin adsorbed layer of an aqueous solution or a molten salt. There is much evidence that this corrosion is not a homogeneous reaction in which the exchange of electrons between the reacting species occurs locally, but rather an electrochemical one, in which a small electric current flows over distances which are large, on an atomic scale. Part of the electrical current circuit is in the metal, and the current takes the form of a flow of electrons, and part of it is in the corrodent, with the current in the form of an ionic drift.

The fact that many important metals, including stainless steels and high-strength aluminum alloys, are subject to SCC in certain environments has long been known (1-7). Either these metals are not used where such cracking might occur, or the conditions of stress, heat treatment, and environment are carefully maintained in order to minimize the likelihood of cracking. Even when SCC occurs in alloys such as type 304 stainless steel or type 2024 aluminum alloy, the results can hardly be described as spectacular. The finale to the process of SCC

in an austenitic stainless steel pressure vessel, for example, is usually simply a leak.

During the 1950's it became evident that some, and perhaps many of the high strength steels being used in large structures, were also susceptible to SCC (8-16). The finale in the SCC process in these steels, unlike the case of austenitic stainless steels, was catastrophic failure. The SCC failure of a pressure vessel made of one of these materials was not a leaking vessel but a shattered one. These failures are apt to be all the more newsworthy because of the nature of the structures which are being made from these steels, or because of structures designers would often like to make out of them. There have been, therefore, in recent years projects seeking to identify those high strength steels which are susceptible to SCC in various environments and to try to determine the condition of heat treatment, stress, and environment under which an otherwise susceptible steel could be safely used.

Data on the susceptibility to cracking by stress corrosion and hydrogen embrittlement were reported (17, 18) for types 410, 420, and 436 stainless tempered at various temperatures in the range 300-1200°F. Beam type specimens were stressed by bending, generally well below the elastic limit and were either exposed to 5% NaCl spray or were arranged as the cathode in a cell containing 0.1 N H_2SO_4 + 3mg As/liter.

The various high-strength steels differ from each other in their resistance to brittle fracture under stress in the presence of a notch; this property, called notch sensitivity, was found in this work to be a function of heat treatments and mechanical properties of Almar 362 steel.

The effect of impressed current on the time to fracture was reported by Brown (19). He impressed external current on bent-beam specimens and recorded the time until a complete fracture occurred. From the nature of these potential-time curves Brown predicted whether the cracking was by stress-corrosion or by hydrogen embrittlement for a specific corrodent.

The Almar 362 mar-aging steel was found to be susceptible to cracking through hydrogen embrittlement as well as by stress corrosion. Potential vs. time curves were obtained in this work during the stress cracking of Almar 362 steel for both hydrogen embrittlement and stress corrosion solutions. It was the purpose of this study to determine the effects of different corrodents and applied currents on the nature of the cracking of bent beam specimens for different strength levels. Metallography and electron microscopy studies were made on specimens cracked under different conditions to determine if microstructural differences between hydrogen embrittlement and stress corrosion cracking could be observed. Since it is known that the susceptibility for stress corrosion cracking increases with an increase in yield strength (20), some of the test specimens were cold rolled before aging, then the time to fracture was determined.

In the present investigation hardness, tensile strength and notch strength measurements were made as a function of aging time, temperature, and corrodent. From these studies it is felt that a more complete understanding of the stress corrosion cracking process in the Almar 362 steel will be possible.

CHAPTER II

LITERATURE SURVEY

Metallurgical Characteristics of Almar 362 Steel

Almar 362 (21) is related to the recently developed nickel maraging steels but contains chromium to give it the corrosion and oxidation resistance of the stainless steels. Control of carbon and residual elements gives the steel unusual toughness and ductility for a martensitic steel. Table 1 is a typical analysis of Almar 362. Further increase in strength is then obtained by a low-temperature aging heat treatment.

The composition balance produces M_s and M_f temperatures well above room temperature. The transformation points are shown in Table 2. Because of the low amount of interstitial elements in Almar 362, a martensitic body centered cubic structure without severe distortion is formed upon cooling to, or below, the M_f temperature. Almar 362 has a low rate of work hardening and good ductility. Due to its low work hardening rate it can be cold worked very severely without resorting to frequent intermediate annealing operations. The alloy is simple to heat treat and has relatively good formability. Its strength is considerably greater than of the annealed 300 series austenitic stainless steels.

In the annealed condition, Almar 362 is fully martensitic, but the martensite is soft and ductile because of control of the carbon

Table 1. Typical Analysis of Almar 362 Steel

Element	Per Cent
C	.035
Mn	.24
P	.016
S	.004
Si	.10
Cr	14.09
Ni	6.70
Ti	1.14

Table 2. Transformation Points

A_3	1490°F
A_1	1160°F
M_s	510°F
M_f	320°F

content and residual elements. Annealing in the range of 1500 to 1650°F can be utilized for intermediate process annealing. Final production annealing, where necessary, may be performed at 1500°F for an hour per inch of thickness.

Almar 362 can be age hardened at 900 to 1150°F after annealing to give room temperature yield strengths of approximately 120,000 to 180,000 psi. Optimum response to aging is obtained by using aging times ranging from eight hours at 900°F to one hour at 1100°F. A desirable combination of strength and toughness is obtained by aging for three hours at 1000°F.

Physical Properties:

Density, .281 lb per cubic inch

Modulus of elasticity, 28,500,000 - 30,500,000 psi

Modulus of rigidity, 11,000,000 - 11,800,000 psi

Poisson's ratio, .293

Almar 362 can be welded by all of the conventional processes used for austenitic stainless steels without pre- or post-weld heat treatment.

The good machinability of Almar 362 in both the annealed and hardened conditions has been demonstrated on automatic screw machine equipment.

Impact strength can be increased by a two-step annealing treatment with only a slight lowering of tensile strength. The machinability of Almar 362 in both the annealed and hardened conditions is good. Unlike many other precipitation hardening steels, Almar 362 machines well in the hardened conditions. Almar 362 can be readily hot and cold

worked using practices and equipment utilized in processing conventional austenitic stainless steels. Forming and hot rolling should be performed using initial hot working temperatures in the range of 2000 to 2250°F.

Almar 362 can also be readily cold worked at room temperature by cold drawing, heading, rolling, swaging, spinning, tube reducing, etc. The heat treatments of Almar 362 are shown in Figure 1.

Annealed Almar 362 has the following range of longitudinal properties:

Ultimate tensile strength, psi 120,000 - 140,000

Yield strength, .2% offset, psi 105,000 - 115,000

Elongation per cent, 10 - 20

Reduction in area per cent, 50 - 70

Hardness, Rockwell C, 22 - 27

Aging at 1000°F ± 25° produces the following range of longitudinal properties:

Ultimate tensile strength, psi 150,000 - 175,000

Yield strength, .2% offset, psi 140,000 - 170,000

Elongation per cent, 15 - 17

Reduction in area per cent, 56 - 65

Hardness, Rockwell C, 33-38

Impact strength ft-lb, 15 - 40

When Almar 362 is annealed, cold worked and then aged, significant increases in tensile strength and hardness can be attained as compared with the properties normally obtained with the conventional annealing plus aging treatments. The reason is that cold working increases the equilibrium concentration (C_d) of defects (22) by decreasing the

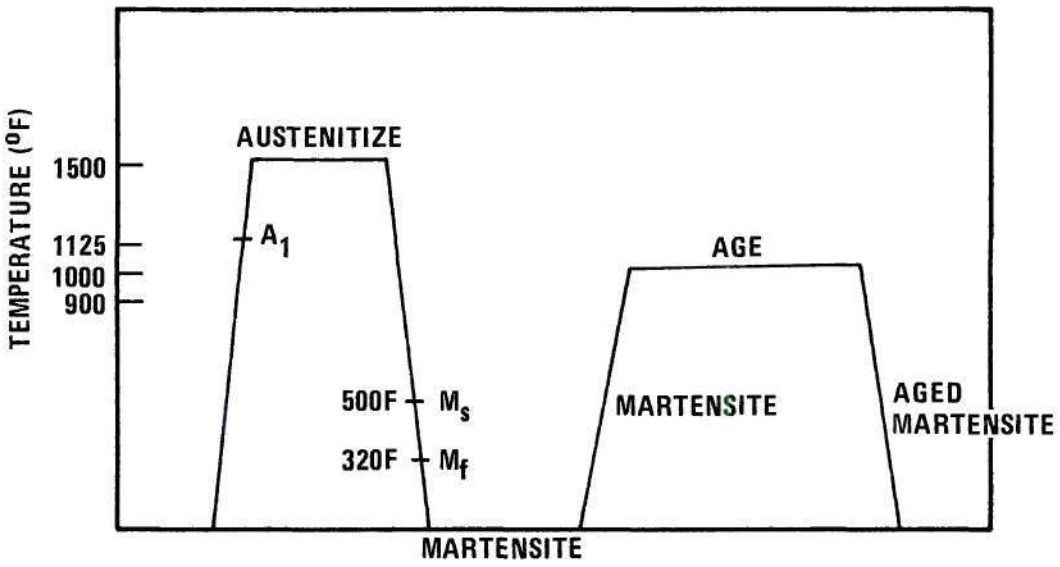

Figure 1. Heat Treating of Almar 362 Steel.

activation energy (U_f) according to the formula

$$C_d = A \exp(- U_f/KT)$$

$$A = \text{constant}$$

The diffusion is accelerated by introducing excess vacancies by cold working. The extent of improvement is related to the degree of cold working and section size or gage.

The fatigue strength of Almar 362 is also important; i.e., a sample annealed at 1500°F for one hour, air cooled, aged at 1000°F for three hours and air cooled, showed fatigue strength 97,000 pounds per square inch at 100 million cycles.

Mechanisms of Stress Corrosion Cracking

There is much disagreement about the mechanisms by which SCC occurs in metals in general. There seems no present justification to complicate an already complex problem by attempting to arbitrarily fit it into a common frame embracing such other phenomena as brittle fracture and cracking by liquid metals. Accordingly, SCC will be reserved here for those cracking phenomena necessarily requiring stress-induced electrochemical corrosion of metal at the advancing tip of the stress corrosion crack; so actually metal goes into solution at the advancing tip of the crack, which by definition is therefore an anode. Simultaneously, electrons are released into the metal, through which they flow to another area of the metal also in contact with the electrolyte. At the second area the electrons participate in a reduction reaction, which by definition makes that area a cathode. The cathodic reaction

may be the reduction of H^+ to H, which may react with dissolved oxygen to form water, form bubbles of hydrogen gas, or dissolve in the metal.

In Figure 2 the cathodic area is shown outside the crack. The propagation of the stress corrosion crack depends upon the flow of the current between the anodic and cathodic areas. If the electrochemical potential of the cathodic areas was adjusted to the potential of the anodic areas, then the driving force of the electrochemical process would be reduced to zero, no current would flow, and the cracking would be expected to stop. This manipulation of the potential can be done by impressing small currents from an external source, and the act is called cathodic protection. This can be effective in stopping, or at least retarding, cracking as has been demonstrated in several systems (8).

Almost all the theory of stress corrosion cracking which has been worked out to date has been derived from experiments with metals other than high-strength steels (23, 24, 25). It seems unwise to assume at this stage that all details of the theory must necessarily apply to the high-strength steels until experience justifies it.

Hydrogen Embrittlement Cracking

If a steel is sufficiently strong and contains more than some minimum amount of nascent H, a sustained tensile load may cause a crack to nucleate and slowly grow at a stress smaller than that required to cause fracture in the absence of hydrogen. This is one manifestation of hydrogen embrittlement cracking (HEC). Lower ductility, higher hydrogen content, and a greater degree of triaxiality of stress enhances this cracking process or diminishes the load required to effect it.

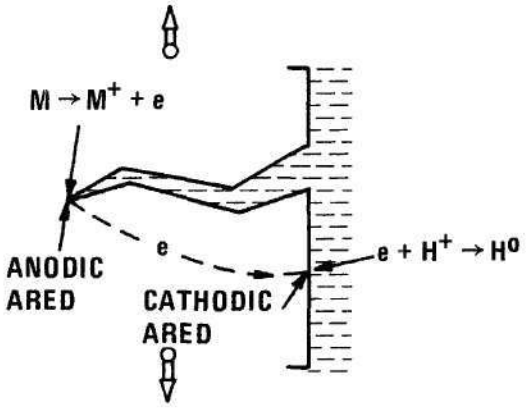

Figure 2. Stress Corrosion Cracking (Schematic).

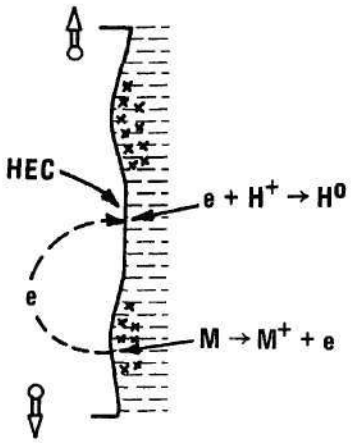

Figure 3. Hydrogen Embrittlement Cracking (Schematic).

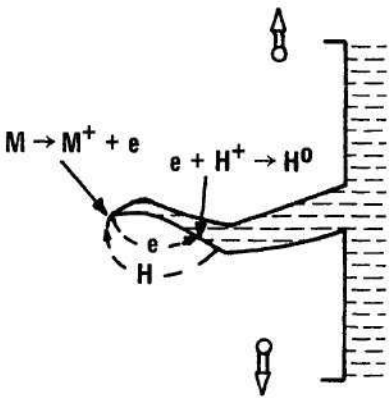

Figure 4. Mixed Cracking Mechanism (SCC and HEC).

Although HEC was explicitly described in the technical literature 30 years ago (17), the basic mechanisms involved are still poorly understood. In common with the special case of SCC, all aqueous corrosion of steel is believed to occur by an electrochemical process in which the oxidation of iron at local anodic areas must be balanced at cathodic areas by an equivalent reducing reaction, which may be the reduction of H^+. If this enters the steel, and if this steel is a high-strength steel under sustained loading, it may experience hydrogen embrittlement cracking. This possibility is illustrated in Figure 3.

There appears to be no reason why this cathodic reaction cannot occur deep within a genuine stress corrosion crack so that both mechanisms of cracking may occur simultaneously or alternately as shown in Figure 4. If one attempts to prevent corrosion of steel in an aqueous solution by applying cathodic protection, he finds that the potential of the steel must be depressed below the potential at which hydrogen can be reduced from the solution. So one of the standard laboratory methods for studying HEC in steels is to cathodically charge them in an aqueous solution. This cathodic charging of hydrogen may be done by an impressed current system, as from a battery.

The procedure used in this work to distinguish SCC from HEC was based on the following criteria:

The term stress corrosion cracking is reserved for cracking in which corrosion occurs at anodic areas at the advancing tip of the crack. Small electric currents flow between local anodes and local cathodes to effect this corrosion. Impressing small cathodic currents from an auxiliary electrode should tend to polarize the local cathode

areas in the direction of the potential of the anodes and thereby tend to mitigate the corrosion and attendant cracking.

Brown (19) has postulated that when a low level cathodic current greatly extends the breaking time, this indicates that the cracking process, in the absence of the impressed current, is properly classified as stress corrosion cracking. On the other hand, when small cathodic currents decrease the breaking time, but the imposition of anodic currents greatly extend the life, this behavior indicates in the case of zero impressed current the failure occurs by hydrogen embrittlement cracking.

When there is no effect of impressing anodic or cathodic currents on the time to failure, this is taken to indicate that the two processes, stress corrosion cracking and hydrogen embrittlement, occur in overlapping ranges of current density.

These electrochemical analyses must be viewed as simplified and preliminary. They are, however, consistent with two subsequent observations: 1) conditions presumed by this analysis to cause SCC indicate the potential behaves as if the cracking were occurring along an active path; and 2) conditions presumed to cause hydrogen embrittlement cracking result in hydrogen permeating a thin iron membrane (26).

CHAPTER III

PROCEDURE

Material

The material used in this study was Almar 362 treated as follows:

1) The strip samples, 1 inch wide and 0.110 inch thick were austenitized for 12 minutes at 1500°F, then cooled separately in air and aged as shown in Table 3. The scale which formed on the surface was removed by grinding down to 0.105 inch.

2) Other samples with the above dimensions were austenitized for 12 minutes at 1500°F and air cooled. The scale which formed on the surface was removed by grinding down to 0.10 inch. The strips were reduced from 0.10 inch to 0.055 inch by cold rolling and then were aged as shown in Table 3.

In both cases the material after aging was cooled in air to retain martensite (aged-martensite).

Mechanical Testing

Ultimate tensile strength was determined by using a Riehle universal testing machine. Hardness was determined by using a manual Rockwell hardness tester.

Stress Corrosion Testing Procedure

After heat-treatment, the specimen surfaces were ground on an 80-grit dry emery belt to remove the heat-treating scale and all

Table 3. Classification of Specimens

Specimen Number	Aging Temperature	Time
No. 1	900°F	8 hours
No. 2	950°F	4 hours
No. 3	1000°F	3 hours
No. 4	1050°F	2 hours
No. 5	1150°F	1 hour

visible surface defects. This treatment was followed by grinding down to 0.10 and 0.05 inch for unrolled and cold rolled material respectively on a 120-grit emery belt. The specimens were then cut to the appropriate lengths to produce the desired stress after bending, degreased in trichloroethylene, washed in distilled water, and rinsed in acetone. The specimens were then stored in a desiccator until the tests were to be initiated.

The appropriate length of the specimen to provide the predetermined stress has been calculated in the Appendix A. The bend stress used was always below the 0.2% offset yield strength of the material. (The range used was from 80% to 95% of the yield strength.) A cross notch was machined in the specimens to initiate the stress corrosion cracking. Specimens were stressed by bending and holding them in the bent position in the holder shown in Figure 5. In performing the bending operation, especially with applied stress approaching yield strength of the steel, over-stressing of the specimen was avoided to stay within the limitations imposed by the elastic analysis (Appendix A).

Anodic-Cathodic Polarization Testing Procedure

External currents were applied to the bent specimens. The impressing current was in the order of a few microamperes/cm^2. A positive current indicated the specimen was being made cathodic; a negative current indicated the specimen was being made anodic.

The test setup is shown in Figure 6. The anode and cathode were from the same material (Almar 362) and had the same surface area for easier control of the current density.

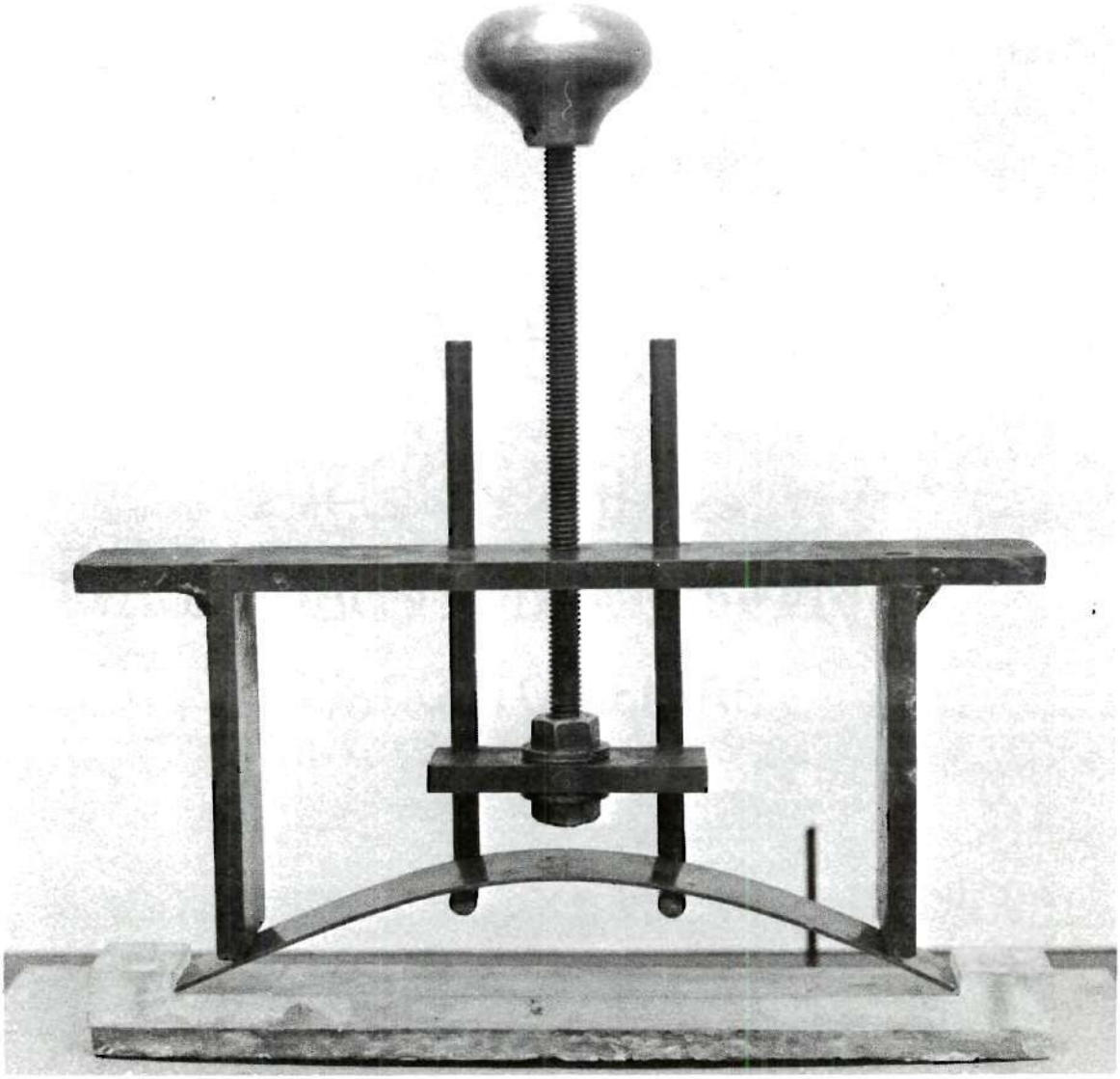

Figure 5. Bending Operation (Schematic).

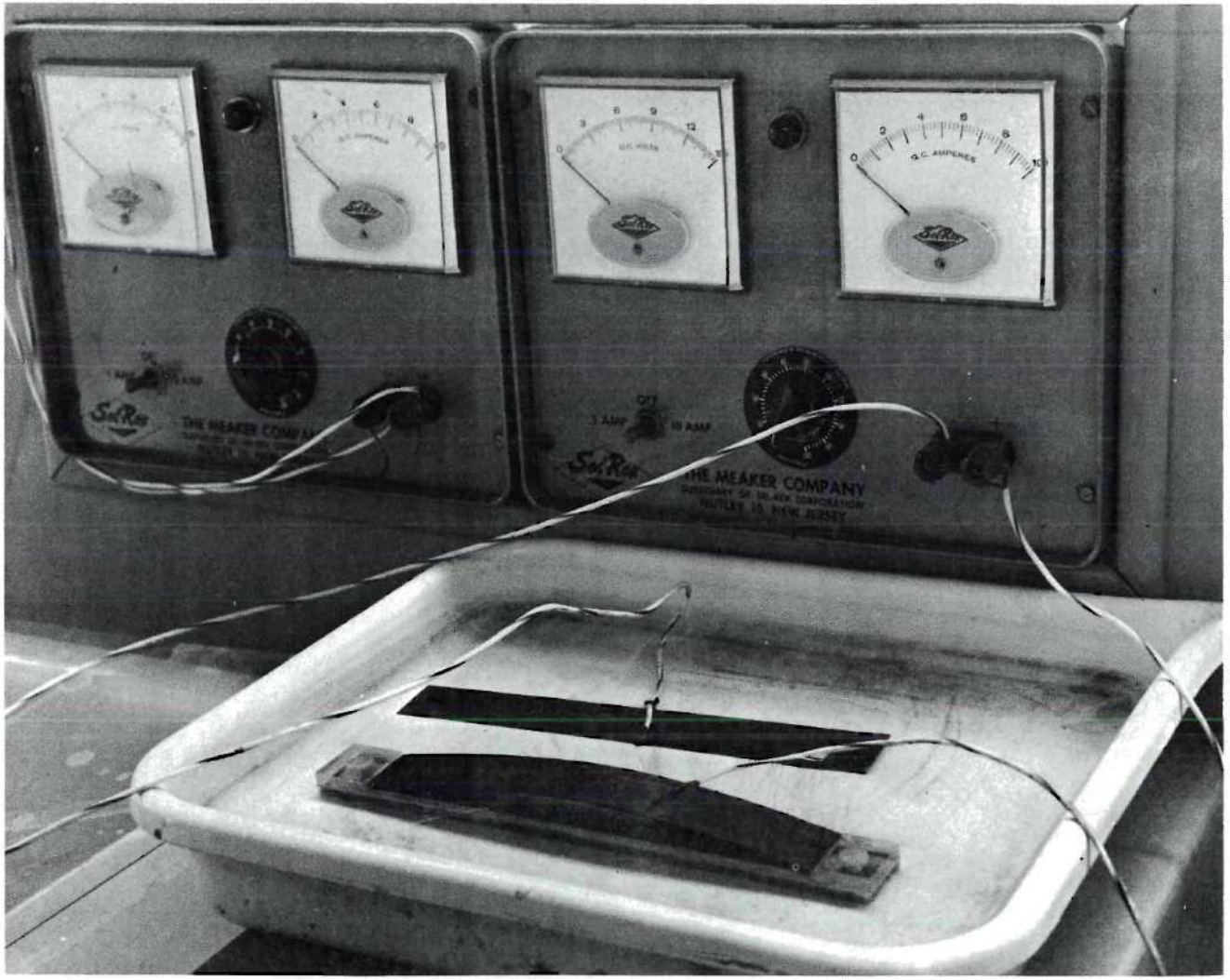

Figure 6. Corrosion Current Apparatus.

A complete description of the results of a stress-corrosion experiment would require a statement of the rate of nucleation and the rate of growth of cracks as a function of stress concentration. This is a formidable task because, among other things, the nucleation and growth of one crack decreases the stress in adjoining areas, which has the effect of tending to inhibit the nucleation and growth of cracks at nearby sites. In this work, only a single parameter of cracking is reported, namely, the total time under exposure until a complete rupture occurred. This, of course, gives a minimum amount of information about the intensity of attack, and it does not distinguish between the incubation time and the growth of the crack which terminated the test.

In the cast of self-stressed bent-beam specimens, the growth of cracks tends to decrease the stress elsewhere in the specimen to the extent that the nucleation and growth of a number of partial cracks may diminish the stresses to the point that no crack propagates entirely across the specimen.

Screening Testing Procedure

The crack toughness of a material, K_c, is defined as the stress intensity factor, K, the value for the onset of rapid crack propagation (27, 28). The measurements to be made are the maximum load and the crack length at onset of rapid fracture. However, it is not really necessary to know the K_c value for very different combinations of values of each of the variables such as heat treatment, temperature, and corrodent.

The main objective in this type of testing program was to establish what combinations of these variables will give the best crack

propagation resistance. This can be done with a screening test which requires less skill and less effort than the K_c determination.

The specimen used was that suggested by the ASTM Special Committee for Progress in the development of crack toughness fracture tests (Figure 7), 1-inch wide with 60° edge notches which are 0.15 inch deep and have root radii of less than 0.001 inch. The corrodent was put around the notches. The measurement made in the screening test was simply the nominal net fracture stress, also called the sharp notch strength (σ_{NS}).

$$\sigma_{NS} = \frac{P}{B(W - 2\alpha_o)}$$

where P is the load, B is the thickness of specimen, W is the width, and α_o is the depth of the notch. The σ_{NS} values have been calculated in the Appendix B.

The difference between σ_{NS} and K_c tests procedure is in the screening test there is no measure of the slow crack growth prior to onset of rapid fracture. The results are usually expressed in terms of the "sharp notch strength ratio," that is, the ratio of the nominal net fracture stress to the ultimate strength.

There is a certain advantage to expressing the results in terms of the ratio of the nominal net fracture stress to the yield strength rather than to the ultimate strength. It is possible to calculate a lower bound of the K_c value from the result of a screening test by using the initial "crack length" rather than the slow crack length, which is not measured. The setup of the screening test is shown in Figure 7.

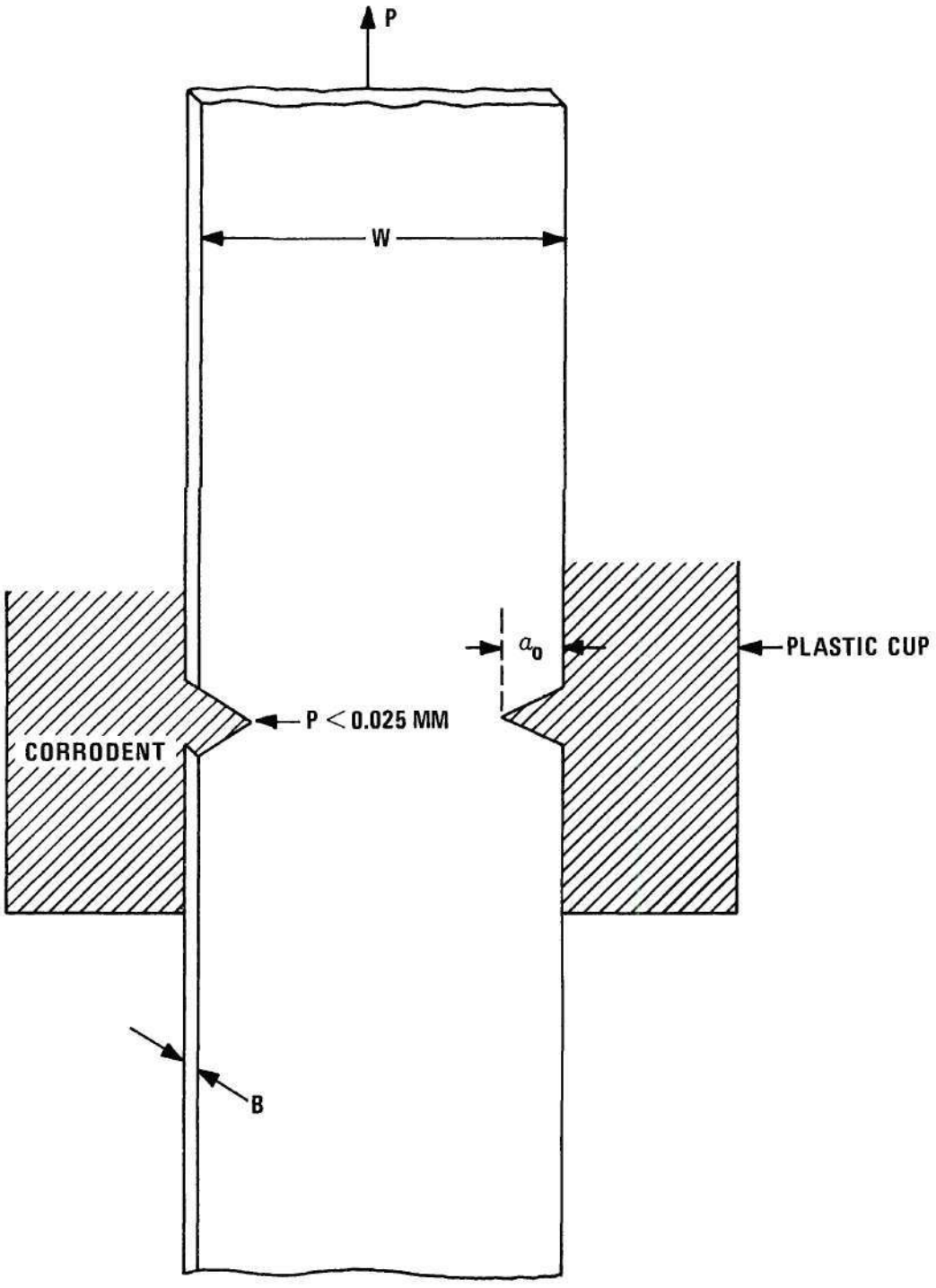

Figure 7. Screening Test Specimen.

Metallography Procedure

Metallographic samples from the cracked areas were mounted in Quickmount and then ground on a wet belt sander. After this the samples were ground on water-lubricated SiC papers from 240 grit through 600 grit. One micron Al_2O_3 and 0.6 micron Cr_2O_3 were used for the final polishing. The samples were then lightly etched with a mixture of 10 per cent HNO_3, 15 per cent HCl, 10 per cent acetic acid, 65 per cent water plus a few drops of glycerin. Electroetching with a 10 per cent chromic acid was also used. Observations were made using a Vickers fifty-five type microscope.

Electron Microscopy Work

During the early days of electron microscopy, several replica techniques were applied to study the nature of the cracking process for both SCC and HEC of high strength steels (29, 30). However, in more recent years with the development of a generally applicable electropolishing technique, a range of high strength steels has been studied.

Electron microscopy was performed on thin foils of Almar 362 steel in order to examine anodically and cathodically cracked samples. The specimens were first chemically etched to a maximum thickness of 3 mils in the following solution:

45 per cent H_2O, 30 per cent HNO_3,
10 per cent HF, and 15 per cent HCl.

After chemical etching, thin foils were prepared by electropolishing, using the following electrolyte:

25 gm CrO_3, 133 ml acetic acid (glacial),
7 ml water.

The edge of the specimen was coated with lacquer for protection against concentrated attack during polishing. The samples were electro-polished using 10-20 volts until holes appeared in the specimen. Data was obtained by using a Phillips EM 200 electron microscope with a metallurgical stage.

CHAPTER IV

DISCUSSION OF RESULTS

Mechanical Properties

The first series of tensile tests was carried out on materials which had been annealed, cold rolled, and then aged. The values of the hardness, ultimate tensile strength, and yield strength are shown in Table 4. The range of values of the ultimate tensile strength, yield strength, and hardness when the material was annealed and then directly aged is shown in Table 5.

We can see that when Almar 362 was annealed, cold worked, and then directly aged, significant increases in tensile strength and hardness were attained as compared with the properties normally obtained with the conventional annealing plus aging treatment. The extent of improvement was related to the degree of cold working and the section size or gage length. The results are shown in Figure 8.

Stress Corrosion Tests

The first data obtained in this work was the variation of the time to failure for bent-beam specimens as a function of heat treatments and bend stresses. Figure 9 shows that the time to fracture increased rapidly with decreasing applied stress. Sample No. 1, which had a 0.015 inch cross notch, bent at about 182,000 psi, then broke after 17 minutes. Sample No. 4, which had a 0.015 inch cross notch, bent at about 144,000 psi, then broke after 6-1/2 days. Since specimen No. 1 was aged at 900°F

Table 4. Ultimate Strength, Yield Strength and Rockwell Rc Hardness for Rolled Material

Specimen	Heat Treatment	Yield Strength 0.2% Offset PSI	Ultimate Strength PSI	Rockwell Rc Hardness
No. 1	Aged 8 hours at 900°F	227,000	240,000	48
No. 2	Aged 4 hours at 950°F	216,000	234,000	45
No. 3	Aged 3 hours at 1000°F	199,000	228,000	42.5
No. 4	Aged 2 hours at 1050°F	181,000	220,000	41
No. 5	Aged 1 hour at 1150°F	145,000	182,000	39

Table 5. Ultimate Strength, Yield Strength and Rockwell Rc Hardness for Unrolled Material

Specimen	Heat Treatment	Yield Strength 0.2% Offset PSI	Ultimate Strength PSI	Rockwell Rc Hardness
No. 1	Aged 8 hours at 900°F	182,000	188,000	44
No. 2	Aged 4 hours at 950°F	172,000	177,000	43
No. 3	Aged 3 hours at 1000°F	160,000	165,000	41
No. 4	Aged 2 hours at 1050°F	144,000	152,000	40
No. 5	Aged 1 hour at 1150°F	115,000	140,000	37.5

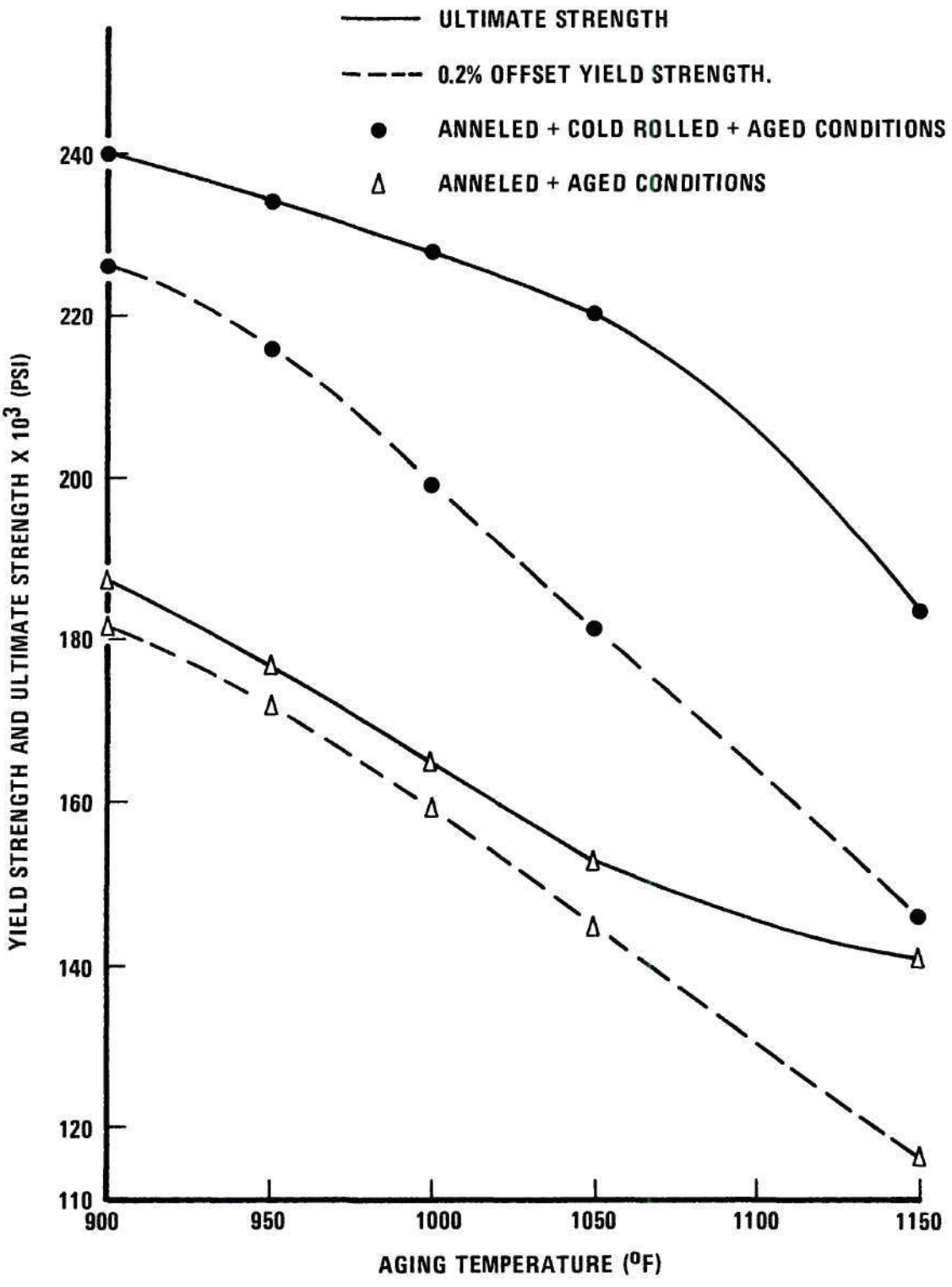

Figure 8. Variation of the Ultimate and Yield Strength in Almar 362 with Ageing Temperature.

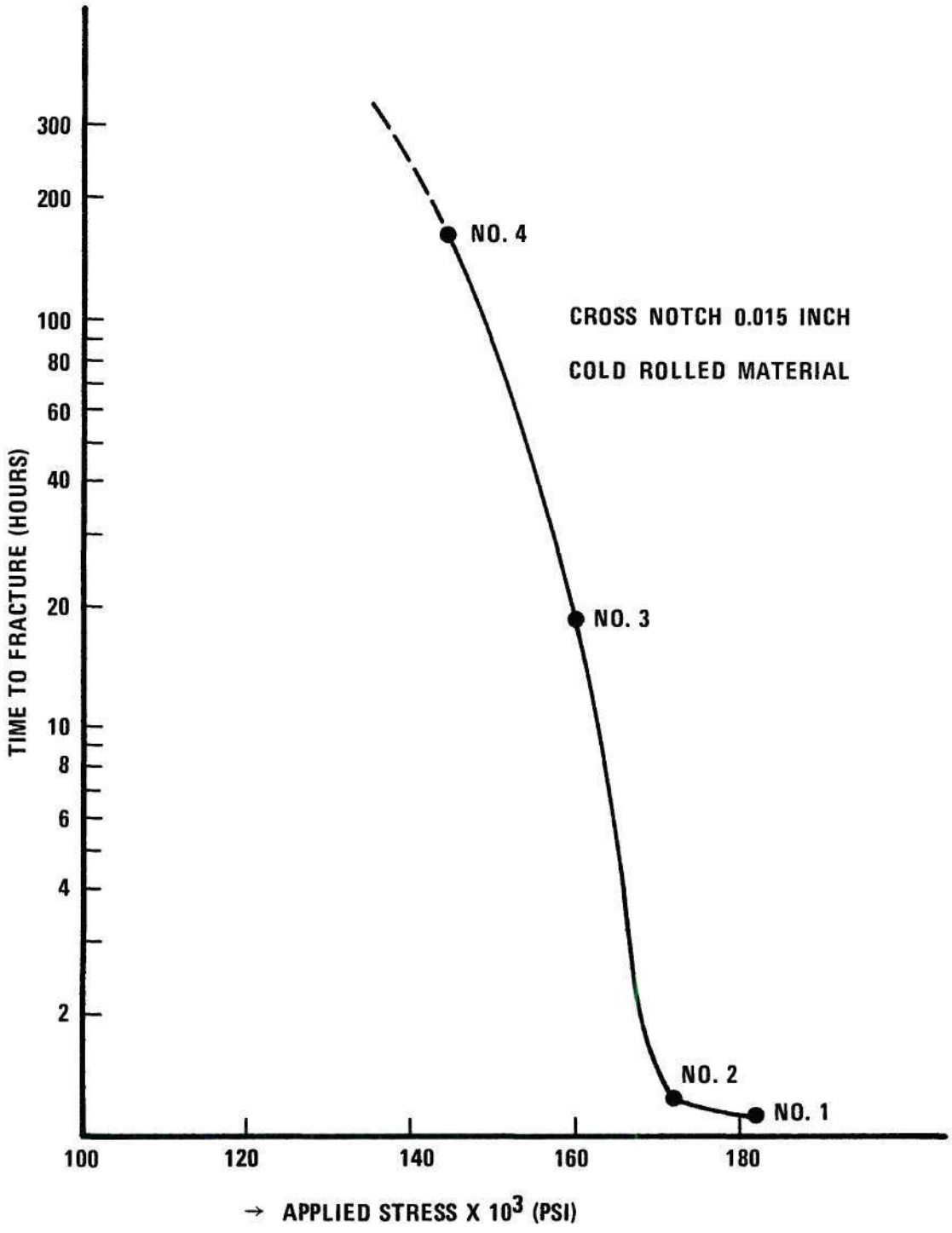

Figure 9. Time to Fracture for Different Specimens (Cold Rolled) Bent at 80% of Yield Strength in a 10% NaCl + 5% HA_c Solution.

and No. 4 at 1050°F, this shows that the Almar 362 had much better resistance to cracking when aged at higher temperatures. Table 6 gives the results of time for failure when the material (annealed, cold rolled, and aged) was stressed in a solution of 10% NaCl + 5% acetic acid. Figure 10 shows the effect of small impressed currents on time to fracture for specimen No. 1.

We can see that when the specimen was made cathodic, the time to fracture was only a few minutes, and when the specimen was made anodic, then the time to fracture increased rapidly above 6 hours. This behavior was taken to indicate that in the case of zero impressed current the failure in a 10% NaCl + 5% HA_c solution occurred by HEC. Figure 11 shows the same behavior for specimen No. 2 in the same solution (10% NaCl + 5% HA_c), that is, again failure occurred by HEC.

Figure 12 shows the same results for specimen No. 3. Here the time to failure was almost 19 hours in the absence of impressed current. When a negative current was impressed the anodic specimen started to dissolve electrolytically and holes appeared in the specimen. These holes introduced stress concentration and made the material weaker; therefore, the anodic current had an opposite effect to the cathodic polarization and decreased the time to fracture. One might also conclude that for positive current the failure occurred by HEC and for negative current the failure occurred by SCC.

A new series of experiments with annealed and aged specimens was performed in bent-beam tests. This material was bent at almost the yield strength (see Appendix A) and put into a solution of 10% NaCl + 8% HA_c. This solution has been chosen because it was experimentally

Table 6. Time to Failure in a Solution of 10% NaCl + 5% Acetic Acid

Specimen	Aging Temperature	Time to Failure
No. 1	900°F	17 minutes
No. 2	950°F	29 minutes
No. 3	1000°F	18 hours and 40 minutes
No. 4	1050°F	6-2/3 days
No. 5	1150°F	no crack after 35 days

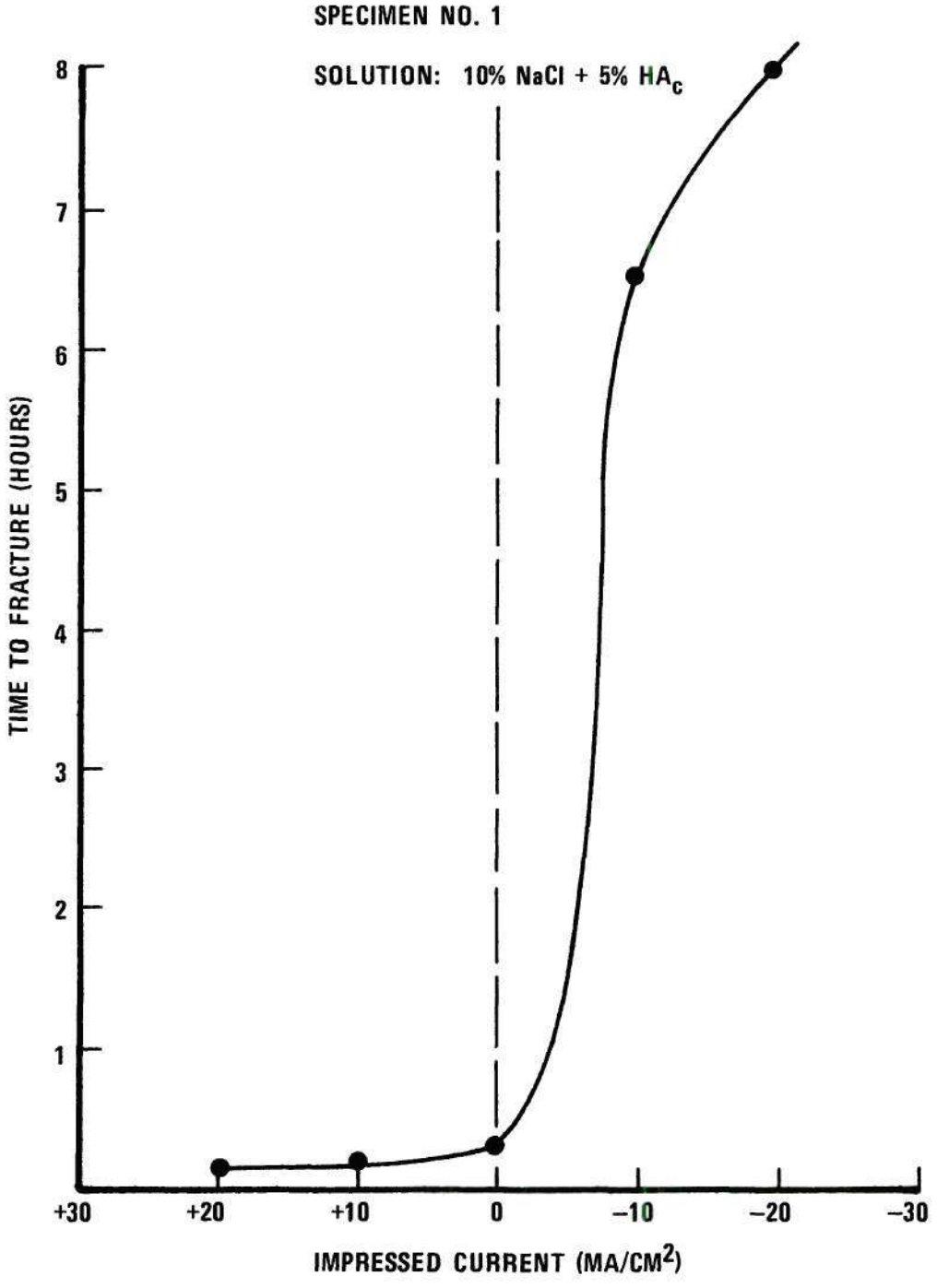

Figure 10. Effect of Impressed Current on Time to Fracture.

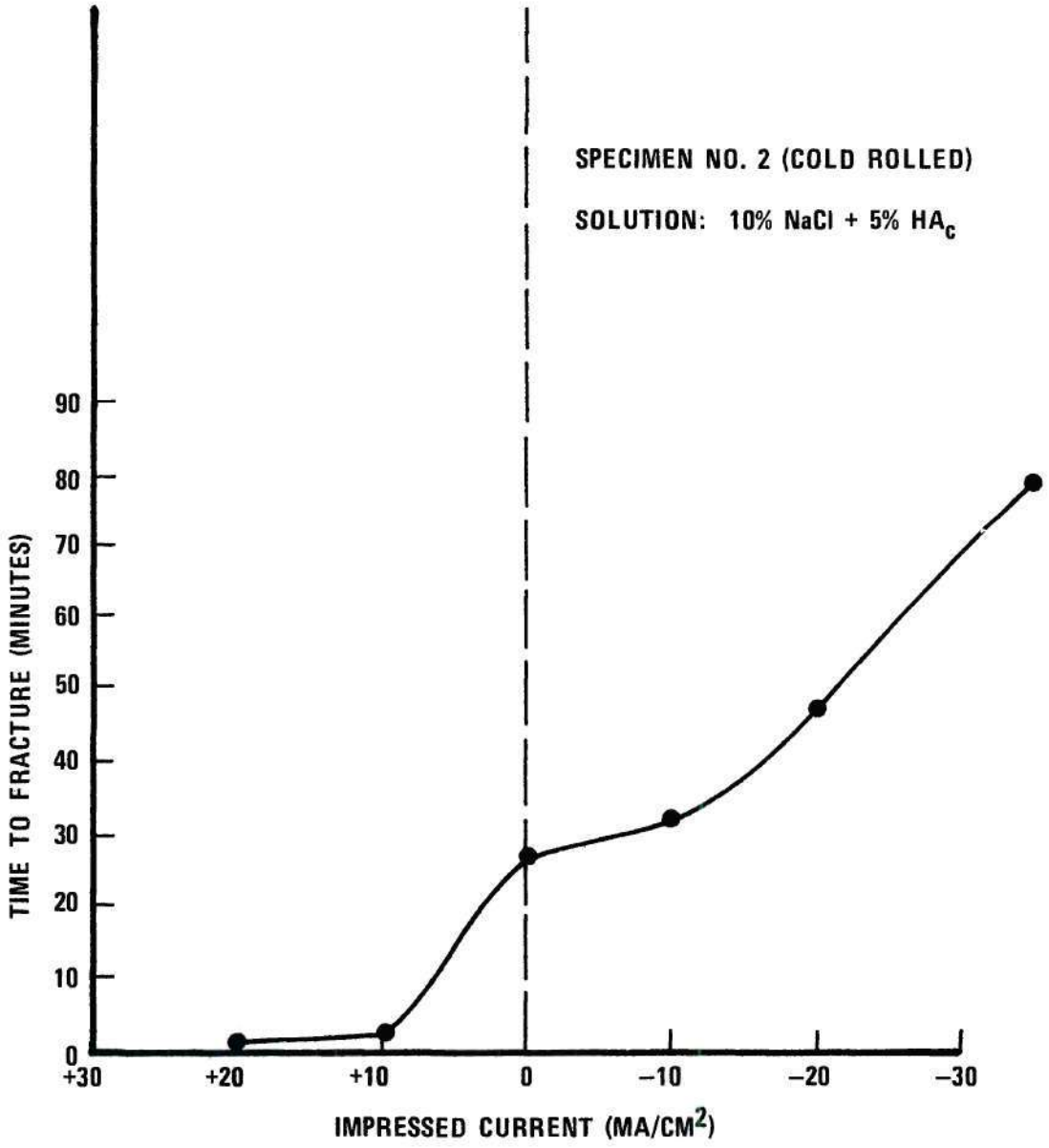

Figure 11. Effect of Impressed Current on Time to Fracture.

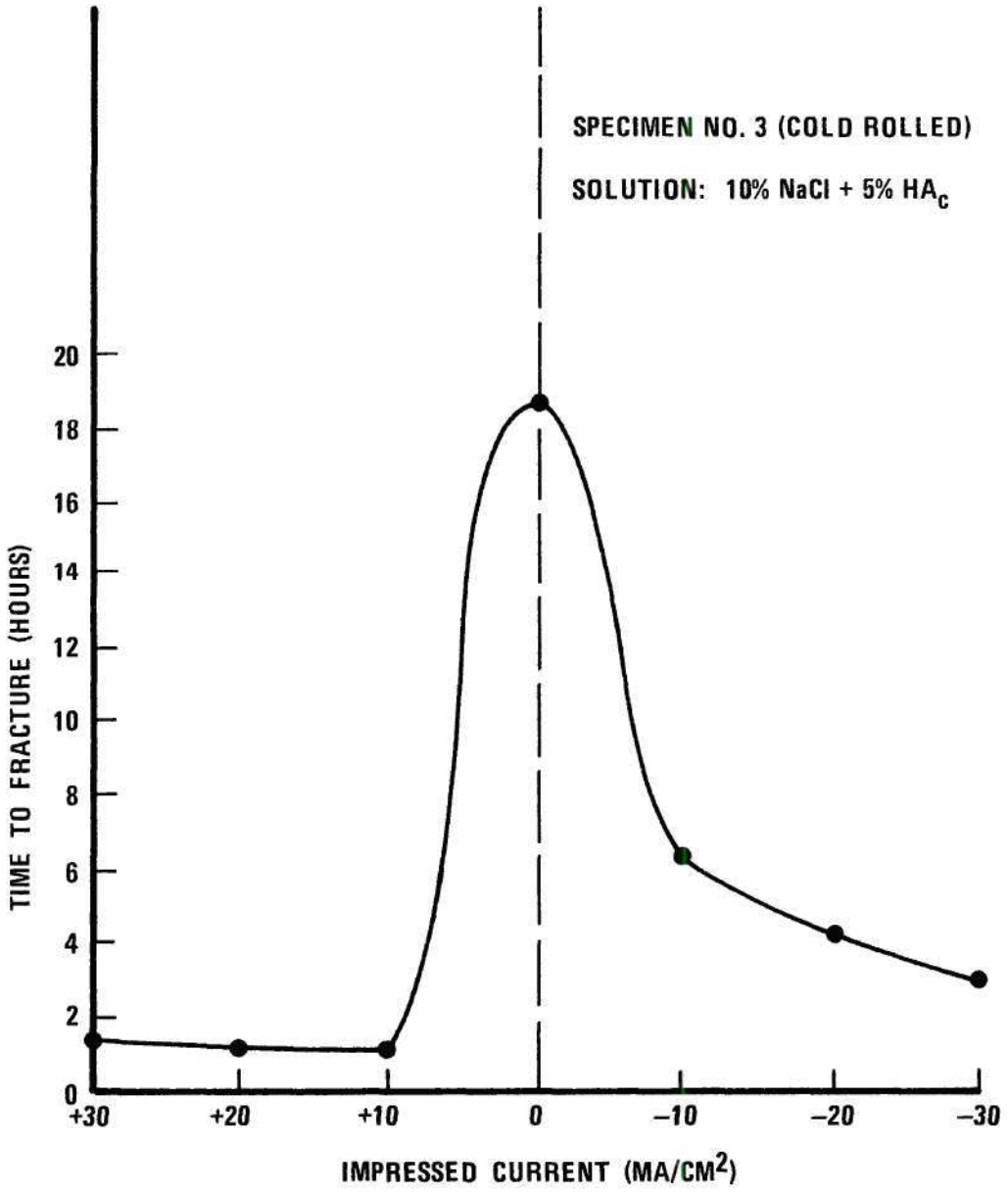

Figure 12. Effect of Impressed Current on Time to Fracture.

determined that pure aqueous NaCl solution did not cause cracking for at least 30 days. It is a significant fact that this steel did not show any significant susceptibility in NaCl solutions of any concentration without catalytic additions. This indicates Almar 362 is quite resistant to most chloride environments. In this test the time to fracture also increased with increasing aging temperature. The results are shown in the Figure 13. By comparison of Figures 9 and 13 we can see that the susceptibility of stress corrosion cracking increased rapidly when the material was cold rolled before aging; for specimen No. 1 the time to fracture was 17 minutes when the material was annealed, cold rolled, and then aged, since the time to failure was 3.5 days when the material was annealed and then aged.

Figure 14 shows the effect of impressed current on time to fracture for unrolled material.

Effect of Selenium Dioxide Upon HEC

Since it is known (31-33) that the presence of SeO_2 in chloride corrodents increases the susceptibility of HEC for steels containing about 14% Cr, it was decided to study the effect of a 50% HCl + 1% SeO_2 solution upon the less susceptible specimens No. 3, No. 4, and No. 5 when the material was rolled before aging, as well as on specimens No. 1, No. 2, and No. 3 when the material was not rolled before aging. Results are shown in Figure 15. From these results it was found that the susceptibility of Almar 362 steel to hydrogen embrittlement cracking was much higher when the corrodent contained SeO_2.

Figure 16 shows the effect of impressed current on the time to fracture of rolled specimens bent in a 50% HCl + 1% SeO_2 solution. Here

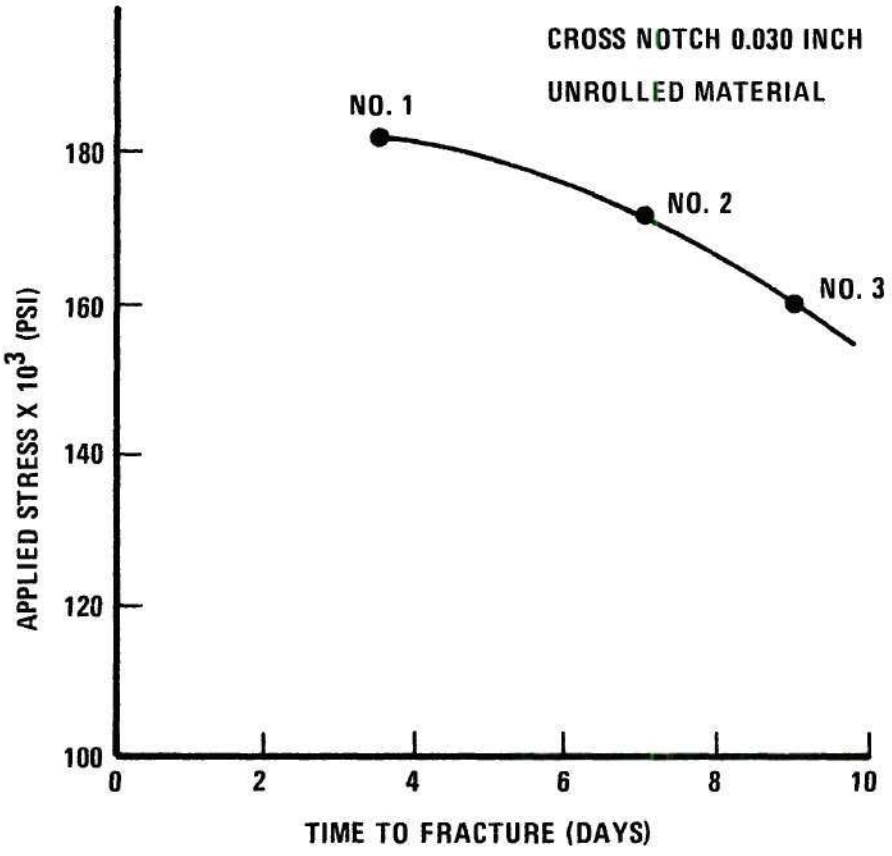

Figure 13. Time to Fracture for Different Specimens, Bent at Yield Strength in a Solution of 10% NaCl + 8% HA_c.

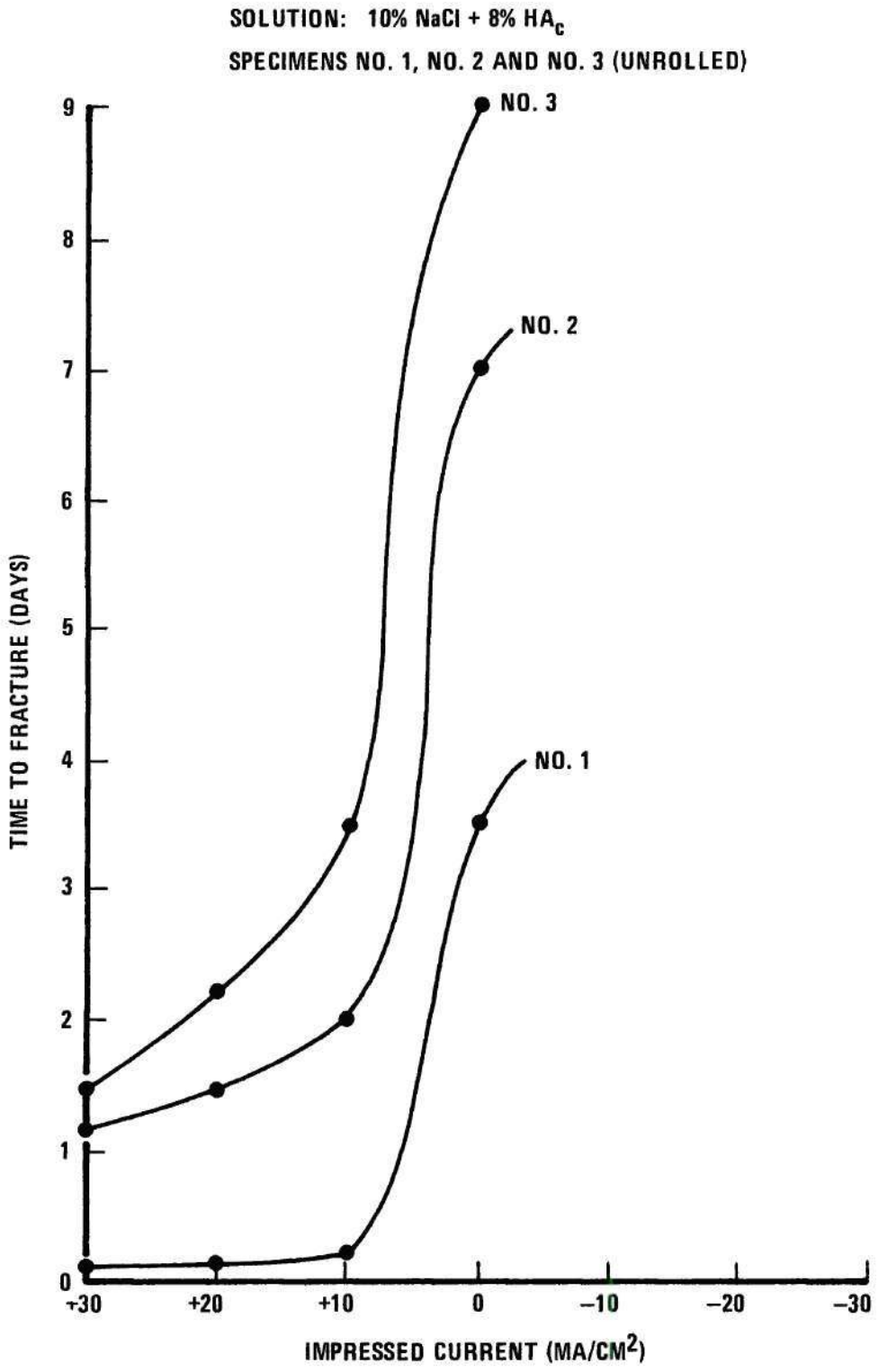

Figure 14. Effect of Cathodic Current on Time to Fracture.

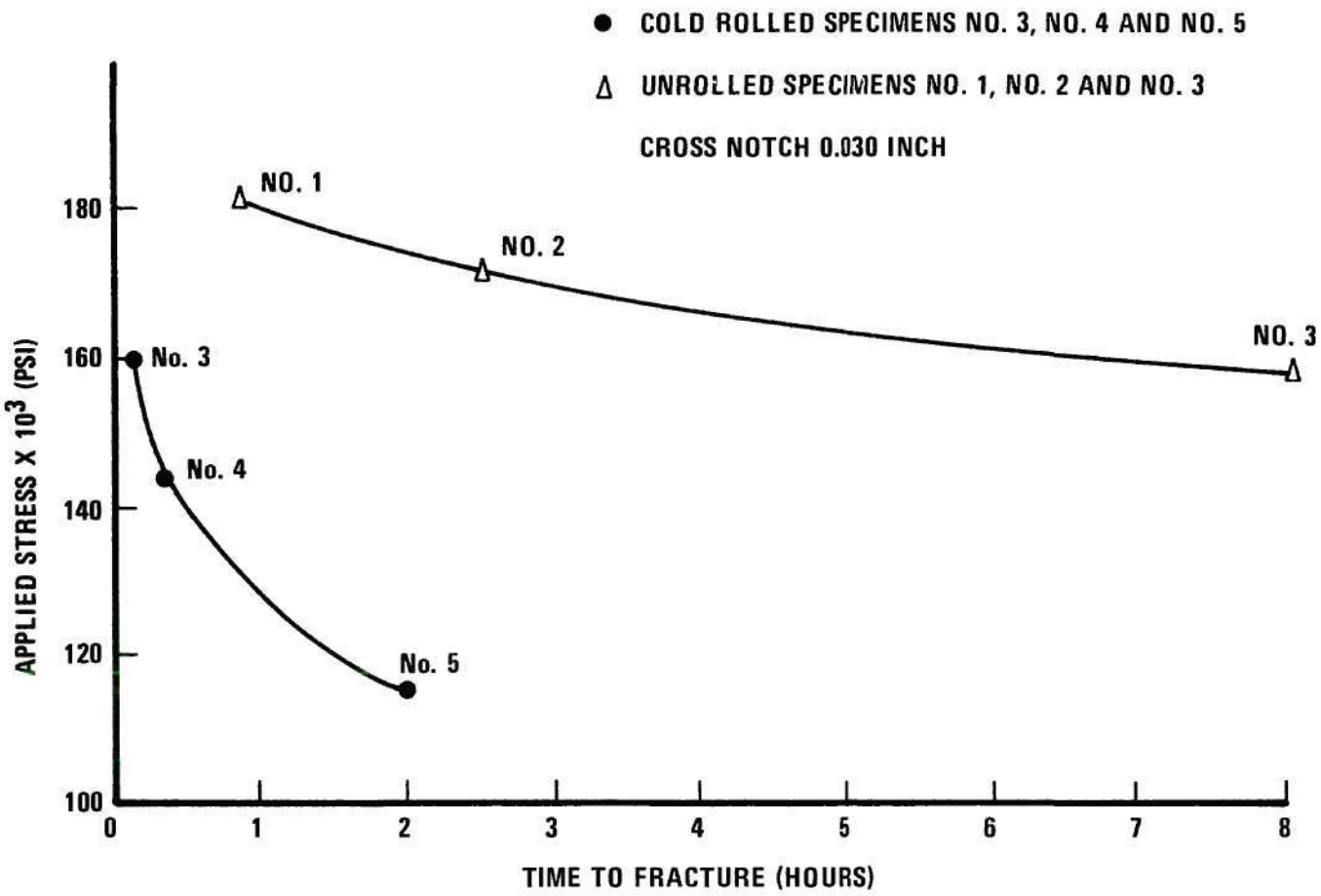

Figure 15. Time to Fracture in a Solution if 50% HCl + 1% SeO_2.

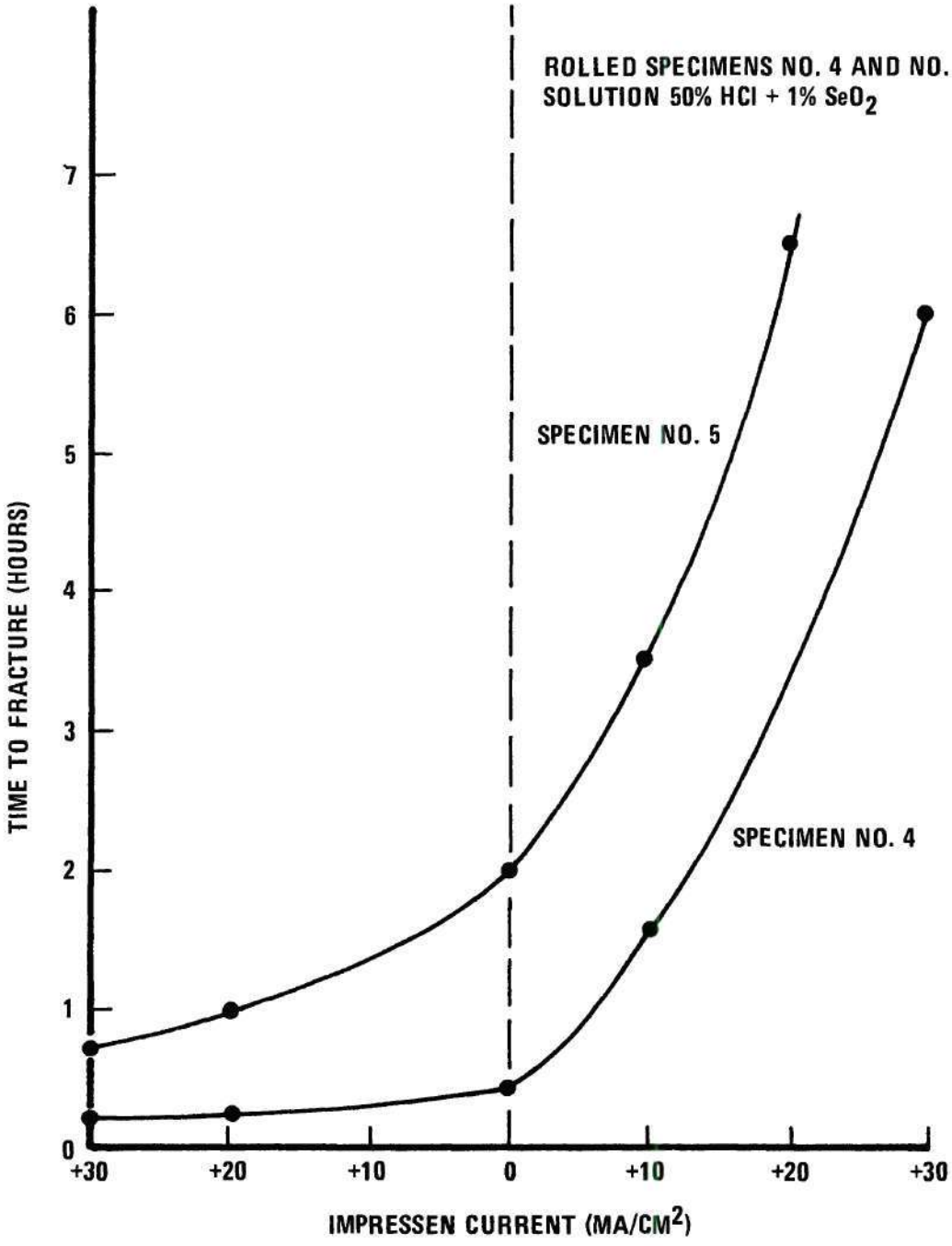

Figure 16. Effect of Impressed Current on Time to Fracture.

the imposition of even a small cathodic current decreased the breaking time, whereas the imposition of anodic current greatly extended the time to failure. This behavior indicates that the failure occurred by HEC.

Figure 17 shows the same behavior of impressed current upon the time to failure for unrolled specimens. When the specimen failed in a SeO_2 solution, there was a sudden rise to a more noble potential (less negative). Cathodic polarization hastened time to failure. Anodic polarization prevented failure but caused pitting and etching attack.

A tentative explanation has been offered for the observed potential changes. To qualify this explanation as tentative there is additional work in progress to test this theory. During the initial change in potential to a more active value, dissolution of metal proceeded fairly rapidly. The cathodic process was predominantly the reduction of selenous acid to selenium metal, which appeared to be catalyzed by the metal surface and deposited there. After the surface was covered by selenium, the potential remained steady or gradually became more noble, depending on the adhesion and porosity of the selenium layer. During this interval, if the surface was scratched and the selenium layer broken exposing bare metal, a repetition of the deposition process occurred in this area. This was reflected by a sudden rise in the potential and subsequent gradual decrease. It was assumed that hydrogen charging became the predominant cathodic process after the surface of the specimen was covered by selenium. As the cathodic polarization was increased, the time to failure after the selenium deposition process occurred was greatly decreased. The actual failure

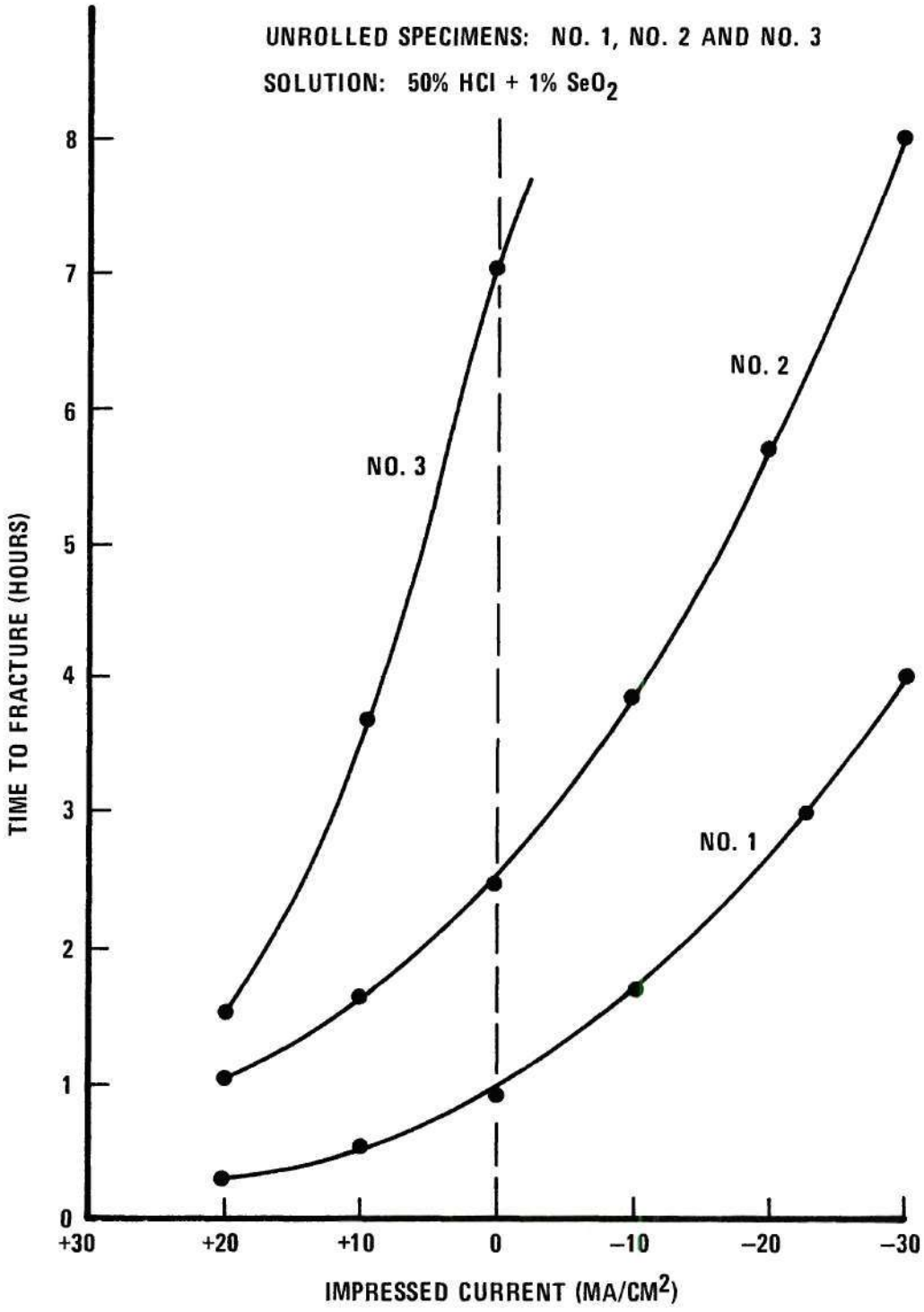

Figure 17. Effect of Impressed Current on Time to Fracture.

of the specimen was mechanical, that is, by hydrogen embrittlement. The reason for the sudden rise in potential was the sudden exposure of bare metal to the corrosive environment.

Screening Tests

Figure 18 shows the effect of the corrodent on a typical screening test. For calculation details of the notch strength (σ_{NS}) see Appendix B.

When the material was not rolled before aging, the effect of the corrodent on the σ_{NS} was insignificant; the corrodent decreased the σ_{NS} values but specimen No. 1 (highest strength) decreased more rapidly than the others. When the material was rolled before aging, the effect of the corrodent on the σ_{NS} was more significant. Again, the σ_{NS} decreased rapidly in specimens of highest strength.

Screening tests were made with the same corrodent but at a higher temperature, 70°C. The solution was stirred constantly while studying the effect of the corrodent on the σ_{NS} values. The corrodent demonstrated a rapid decrease in σ_{NS} values as is shown in Figure 19. This is the result of the increasing reactivity of the corrodent accompanying the temperature increase and the stirring.

Metallography Results

Fracture faces of all specimens were examined optically. A photomicrograph of the mode of fracture is shown in Figures 20, 21, and 22. It was noted that material had apparently been removed from the cracks by the corroding solution as evidenced by the rounded, wide nature of the crack. This dissolution effect was not caused by the

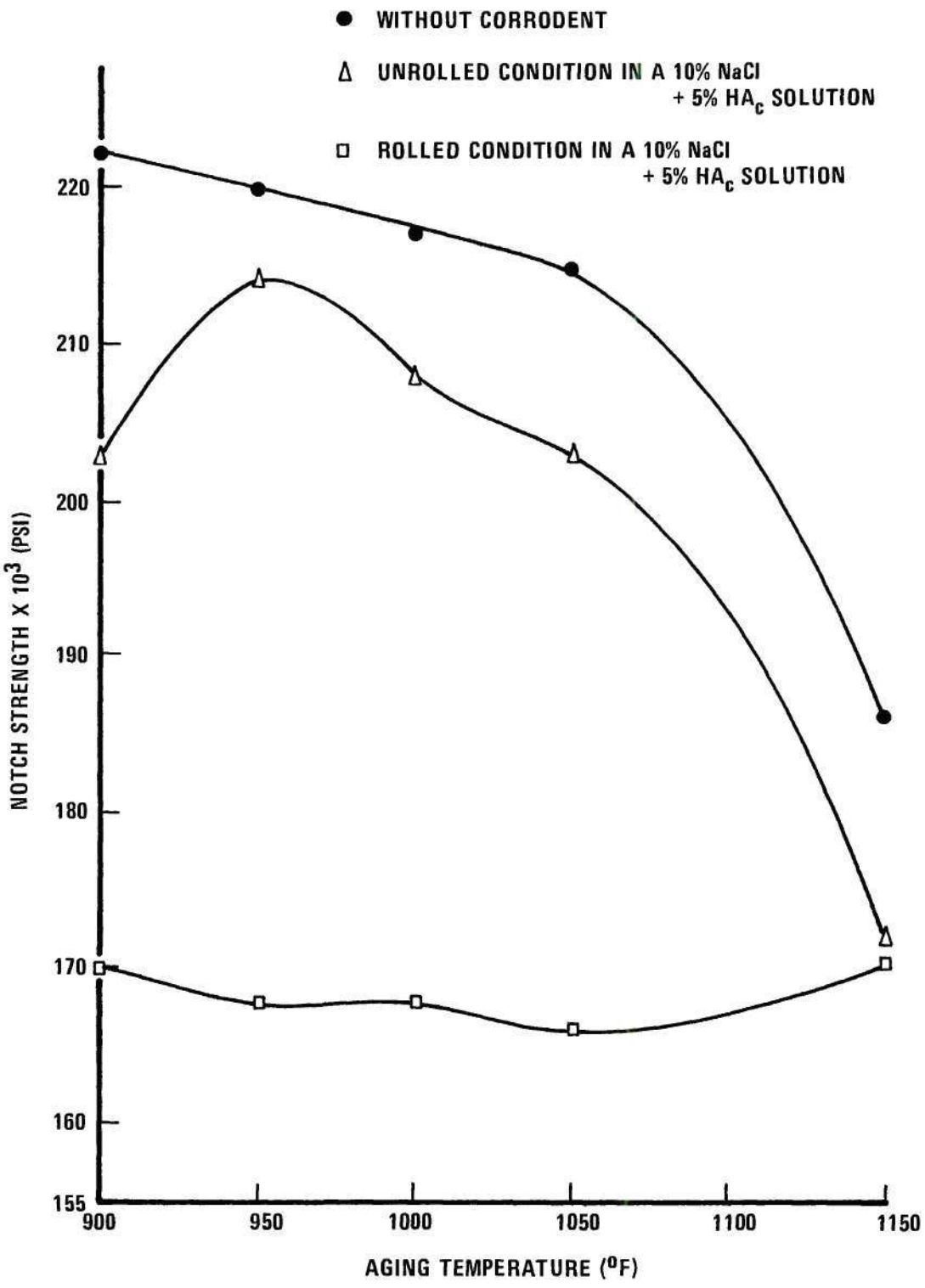

Figure 18. Effect of Corrodent on Notch Strength at 25°C.

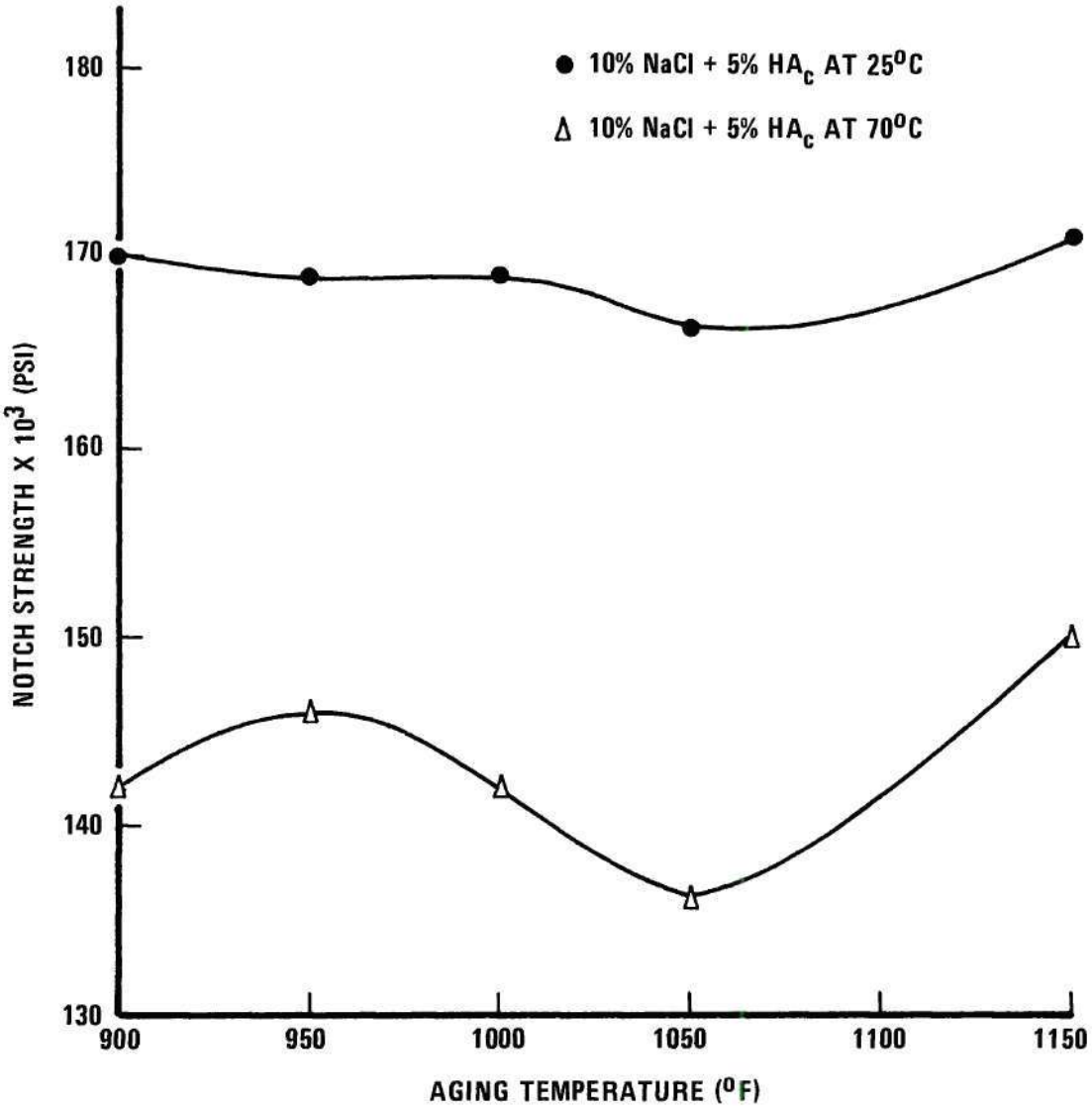

Figure 19. Effect of Corrodent on Notch Strength at 70°C.

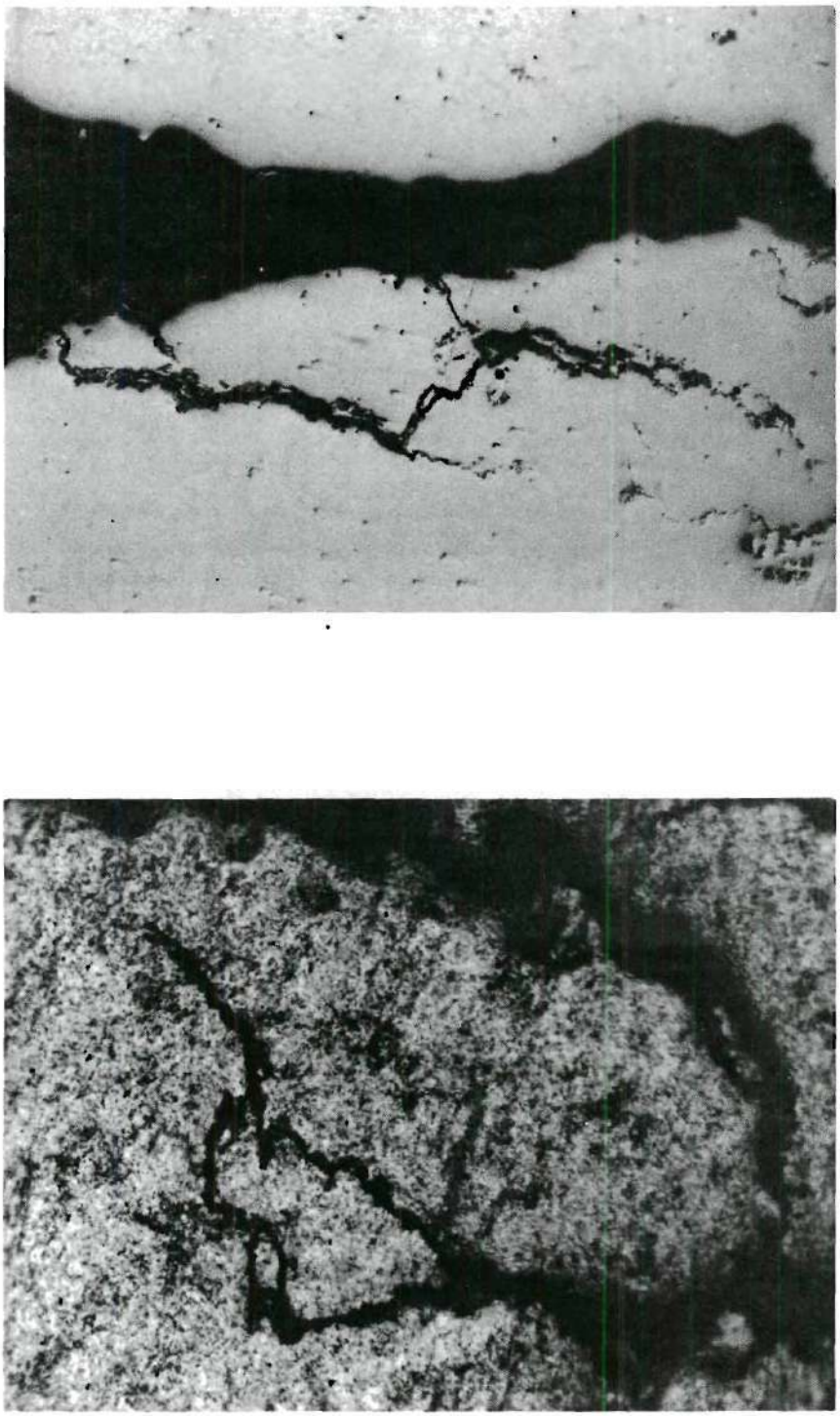

Figure 20. Typical Crack in Almar 362. Bent Specimen Made Cathodic in a 50% HCl + 1% SeO_2 Solution (a Unetched, b Etched, Magnification 400X).

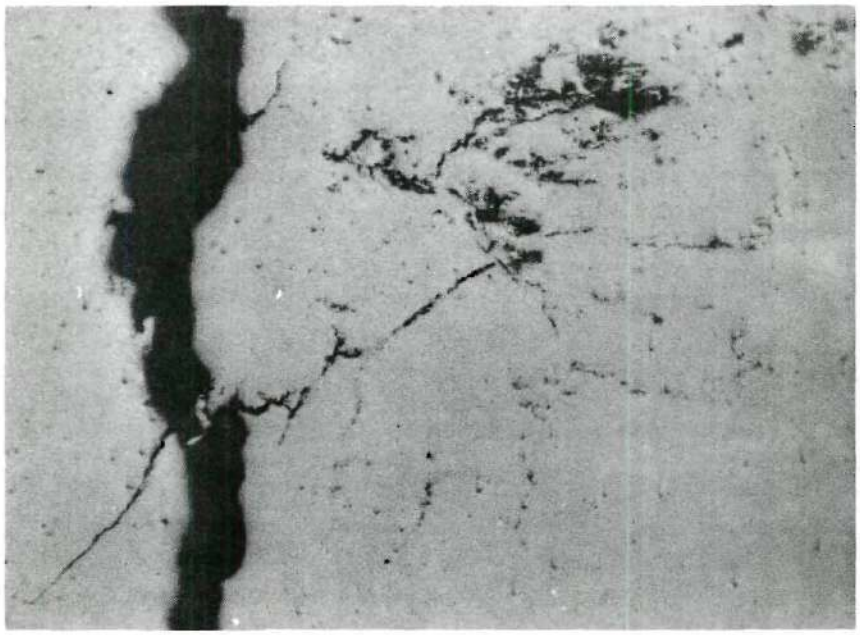

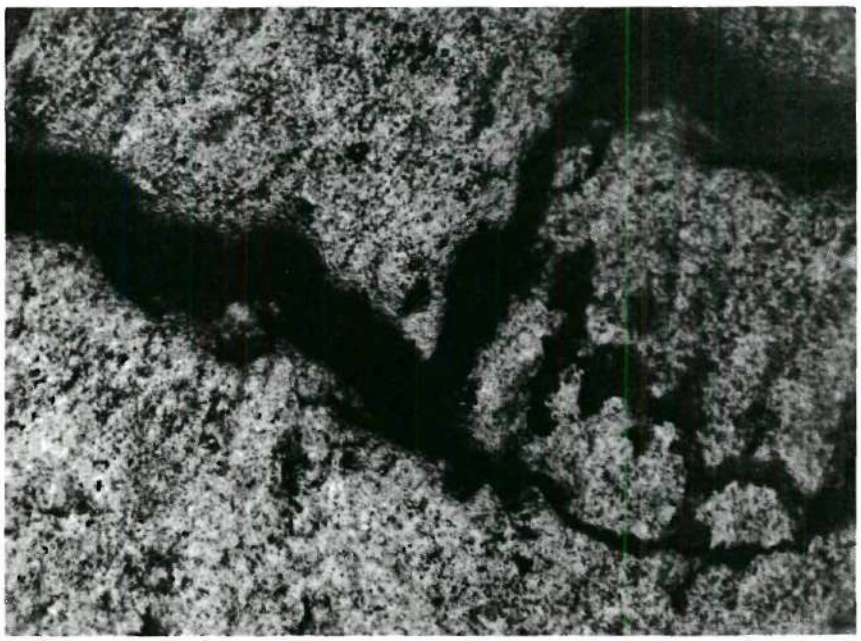

Figure 21. Typical Crack of Bent Specimen Made Cathodic in a 50% HCl + 1% SeO_2 Solution (a Unetched, b Etched, Magnification 400X).

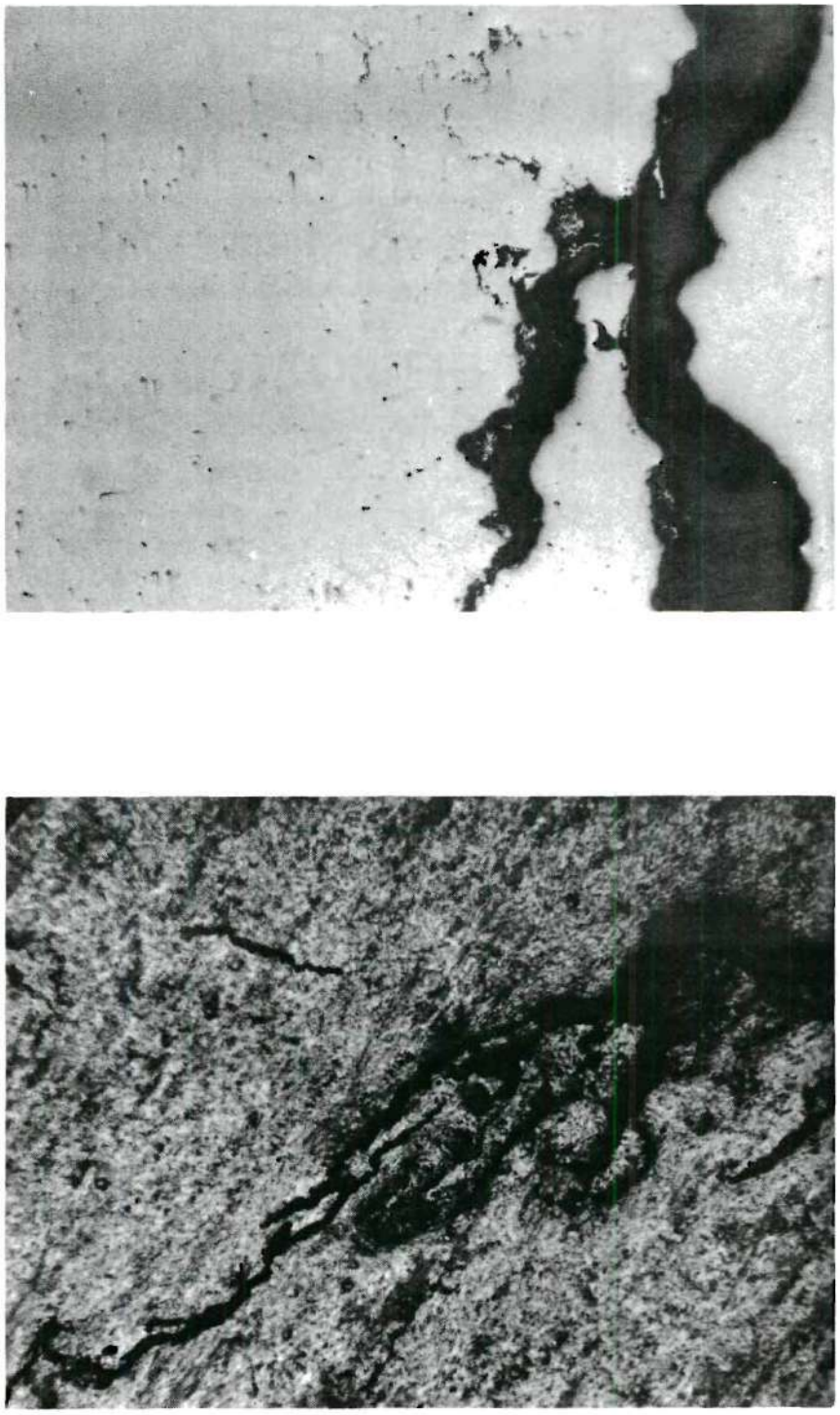

Figure 22. Typical Crack in Almar 362. Specimen Made Anodic in a 50% HCl + 1% SeO_2 Solution. (a Unetched, b Etched, Magnification 400X).

metallurgical etching procedure because unpolished specimens also showed this condition. The fan-like spread of the cracks from the pit locus might be attributed to hydrogen embrittlement of surrounding metal. Loginow (34, 35, 36) observed with 12 Mo.V stainless steel in sodium chloride solution that branching cracks occurred with anodic polarization but that there was no branching with cathodic polarization. It was hoped that with anodic-cathodic testing in Almar 362 a metallographic criterion could be developed to differentiate between hydrogen embrittlement and stress-corrosion cracking. Such a technique would be invaluable in failure analysis. But in Almar 362 branching cracks occurred, both by anodic and cathodic polarization tests supporting the idea that in such a steel both processes are fundamentally related. Branching cracks, not very pronounced, were also found by E. Davis (29) in 4330 and 4340 steel, both for anodic and cathodic polarization.

It was difficult to assess the actual nature of the cracking because none of the recommended etching media was able to reveal the prior austenite grain boundaries.

The metallographic data of Almar 362 steel showed no evidence of a difference in anodic and cathodic cracking.

Scanning Electron Microscope (SEM) Studies

Scanning electron microscopic observations were made on fractured areas of Almar 362 steel using a Cambridge stero-Scan Mark IIA. These studies were restricted to material aged to maximum hardness.

It was hoped that with SEM studies a fractography criterion could be developed to differentiate between anodic and cathodic cracking;

this technique provides for the direct examination of surfaces with a depth of focus nearly 300 times greater than optical microscope, with a resolution approaching 100Å and so the (SEM) has unique capabilities for the study of fracture surfaces.

Figures 23 to 27 show scanning electron micrographs from specimens cracked in air in a 10% NaCl - 5% HA_c solution and in the same solution with cathodic and anodic impressed current.

Figure 23 shows a fracture surface of a typical tensile tested specimen; here the ductile nature of the fracture is pronounced. Figure 24 shows a fracture in a 10% NaCl + 5% HA_c solution without any impressed current. The fracture has the appearance of quasi-cleavage. In Figure 25, cathodically cracked specimen, the cleavage appearance of the fracture is clearly observed across the specimen starting at the top right hand corner close to the machined notch; however, the final fracture area on the left side is of a ductile nature. From Figures 25 and 26, both cathodically cracked specimens, the fracture seems to be transgranular cleavage although some areas may show indication of intergranular failure. Figure 27, anodically cracked specimen, also shows some cleavage appearance, here the corrosion attack is more pronounced because anodic polarization caused attack of the crack surface; this fracture looks more transgranular.

In general, scanning electron microscopy studies showed slight difference between anodic and cathodic cracking and are in good agreement with conclusions drawn from the optical and electron microscopic studies.

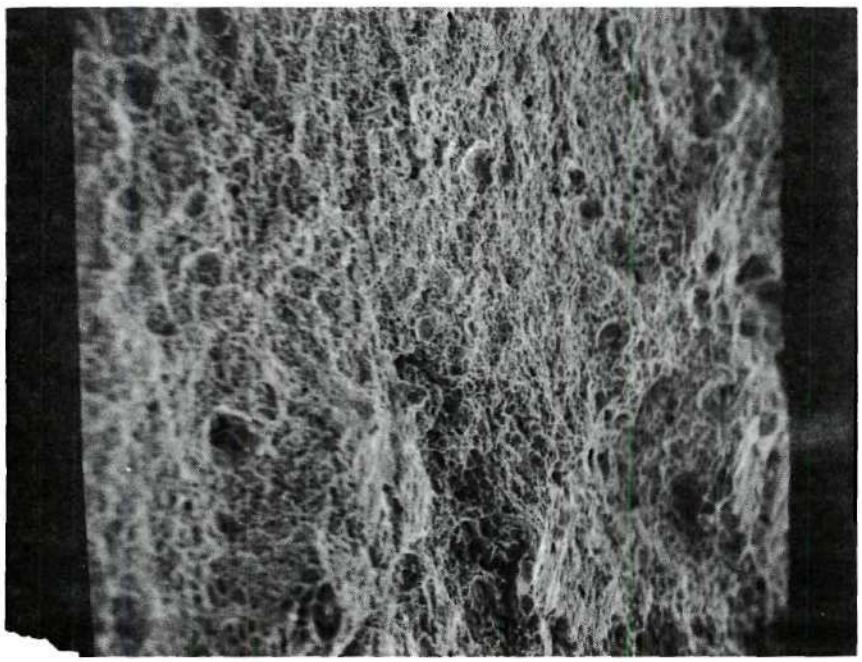

Figure 23. Scanning Electron Micrograph. Specimen No. 1 Cracked in Air (Magnification 1100X).

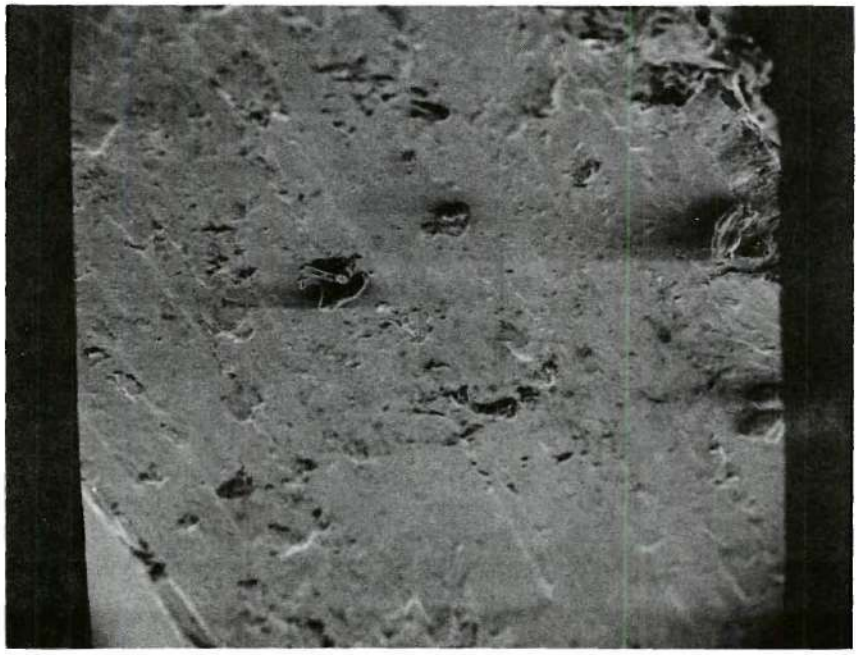

Figure 24. Scanning Electron Micrograph. Specimen No. 1 Cracked in a 10% NaCl + 5% HA_c Solution (Magnification 260X).

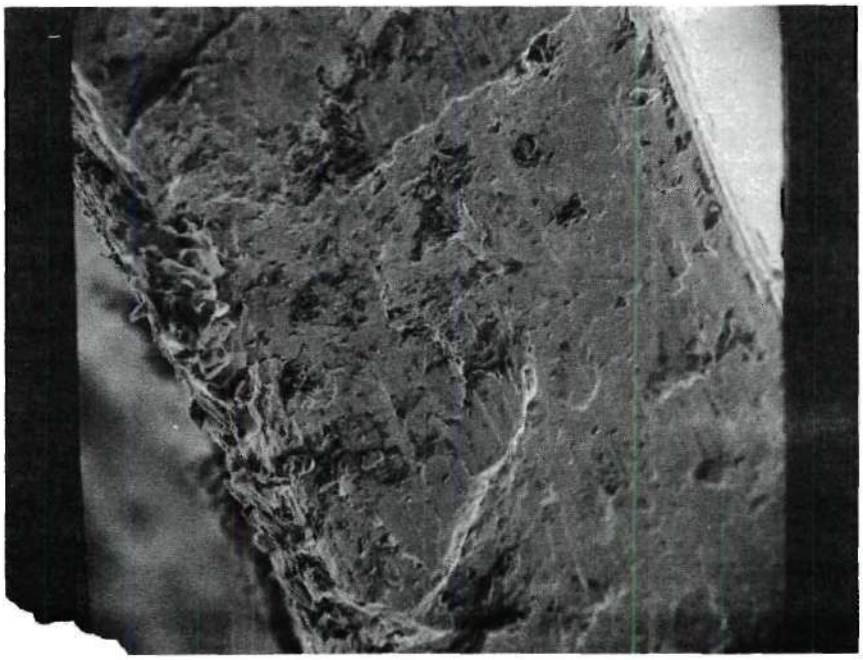

Figure 25. Scanning Electron Micrograph of Almar 362. Specimen No. 1 Made Cathodic in a 10% NaCl + 5% HA_c Solution (Magnification 220X).

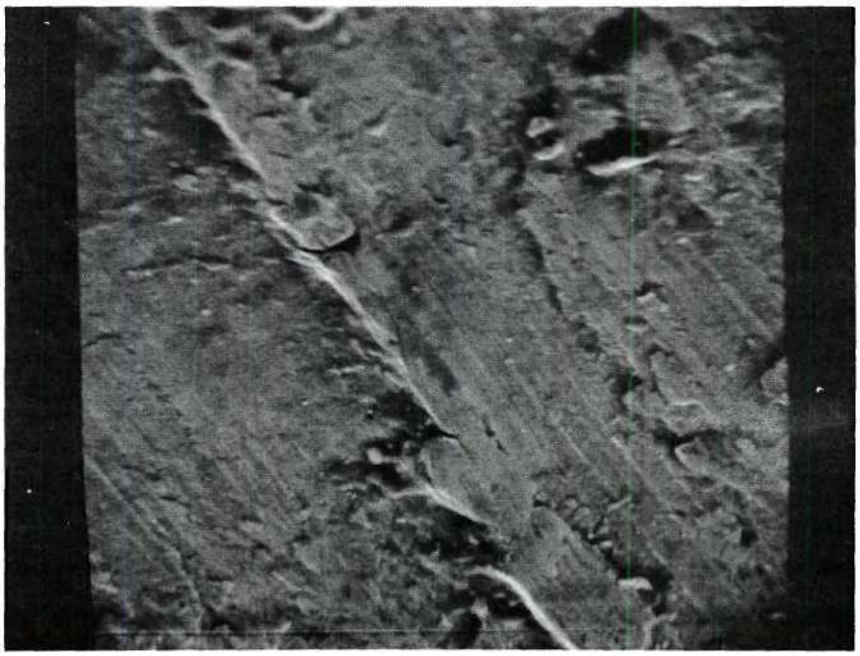

Figure 26. Scanning Electron Micrograph. Specimen No. 1 Made Cathodic in a 10% NaCl + 5% HA_c Solution (Magnification 2400X).

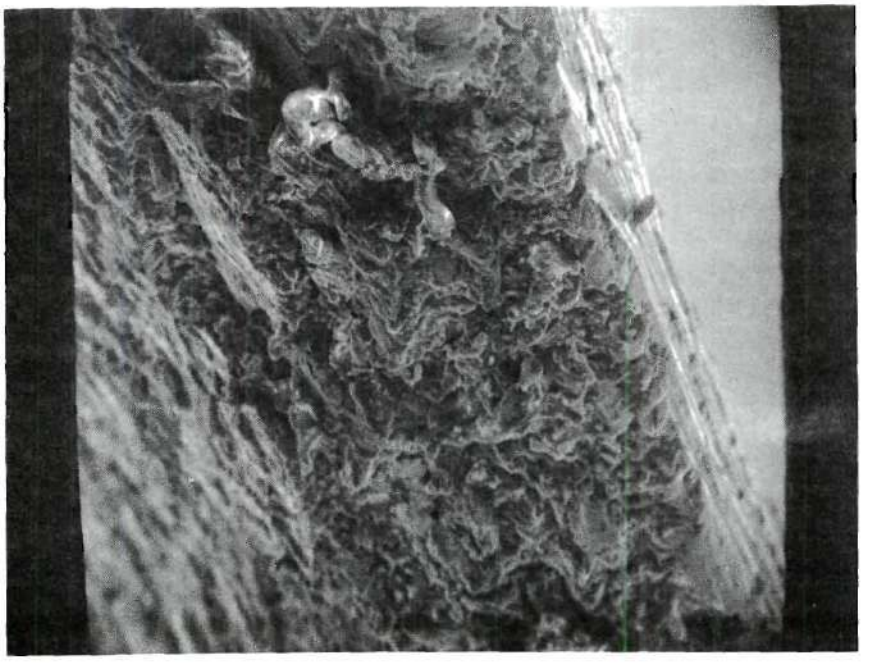

Figure 27. Scanning Electron Micrograph. Specimen No. 1 Made Anodic in a 10% NaCl + 5% HA_c Solution (Magnification 520X).

Transmission Electron Microscopy Studies

The electron microscopic observations were made of thin foils of Almar 362 steel using a Phillips EM 200 electron microscope with a metallurgical stage. These studies were restricted to material aged to maximum hardness.

Figures 28 to 33 show transmission electron micrographs from specimens anodically and cathodically cracked. These pictures demonstrate identical microstructure adjacent to the crack in both cracking processes. Many precipitates were seen and there was a marked tendency for these precipitates to be in the grain boundaries.

The contrast at the grain boundaries was complex; in some cases individual dislocations appeared to be resolved, but in general it was difficult to be certain that individual dislocations rather than interference fringes were being observed. To elucidate the structure of a particular boundary, observations of contrast change with tilting together with electron diffraction data from the area involved would be required.

The precipitates were clearly visible in the vicinity of extinction contours. The contrast effects associated with the precipitates were very unusual. It was observed that dark patches of contrast, which often overlapped, surrounded the precipitate particles. This contrast was believed to be a result of the deformation producing cold strain in the matrix around the particles. The structure which was observed corresponds to an aged state near maximum hardness where the strain fields have become nearly continuous between precipitate particles. The extensive cold worked strain contrast made it difficult

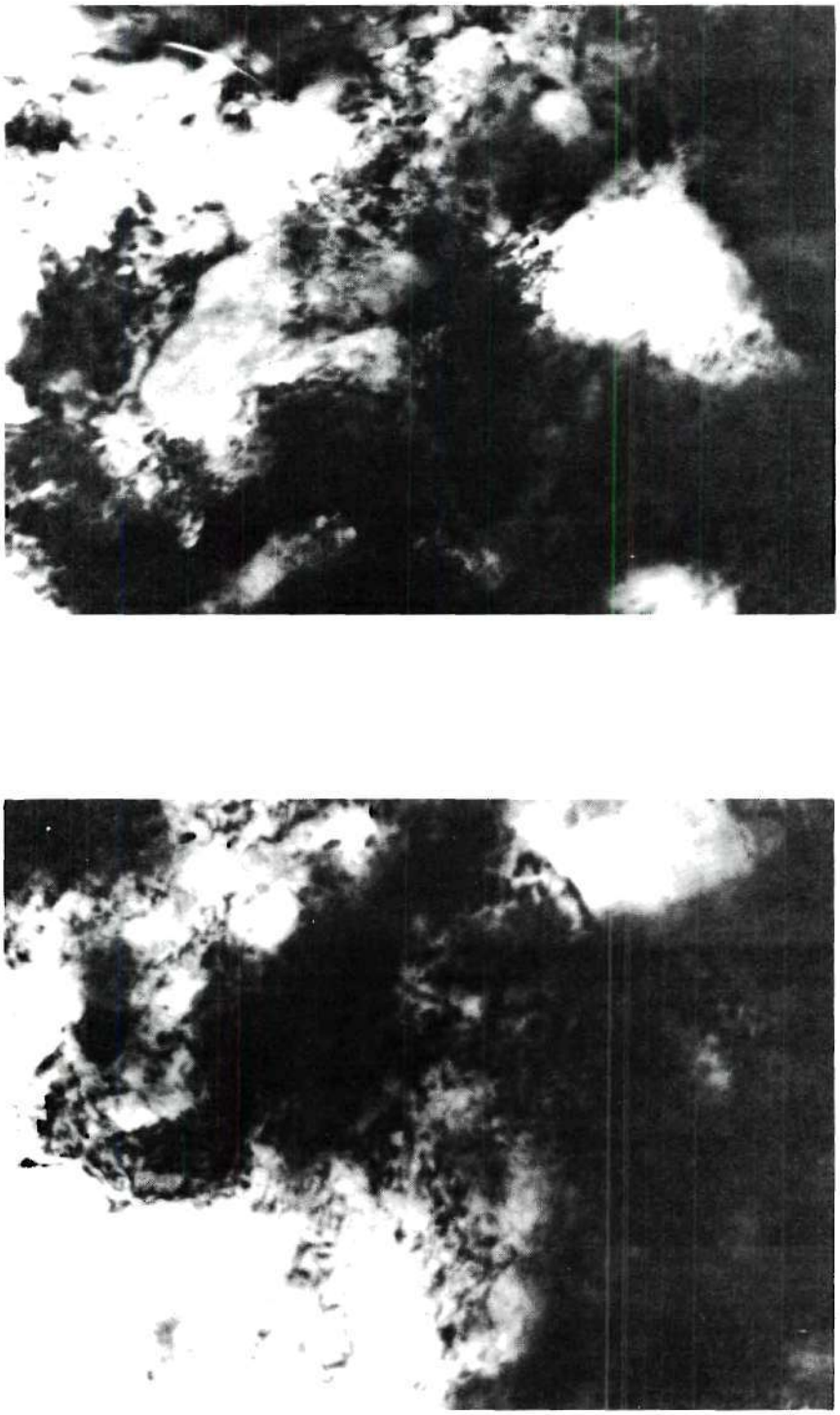

Figure 28. A Transmission Electron Micrograph of Almar 362. Specimen No. 1 Made Anodic in a 50% HCl + 1% SeO_2 Solution.

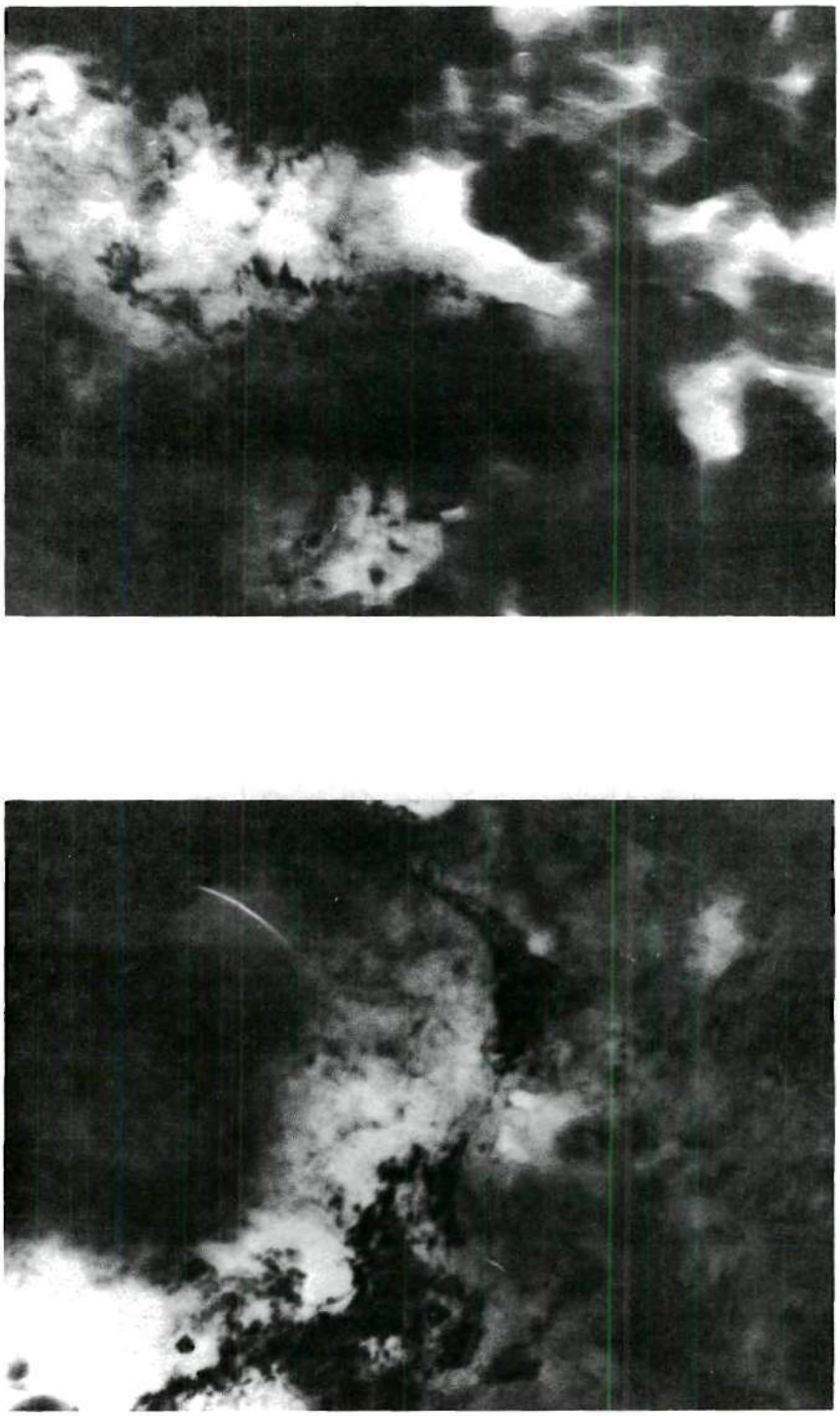

Figure 29. A Transmission Electron Micrograph of Almar 362. Specimen No. 1 Made Anodic in a 12% NaCl.

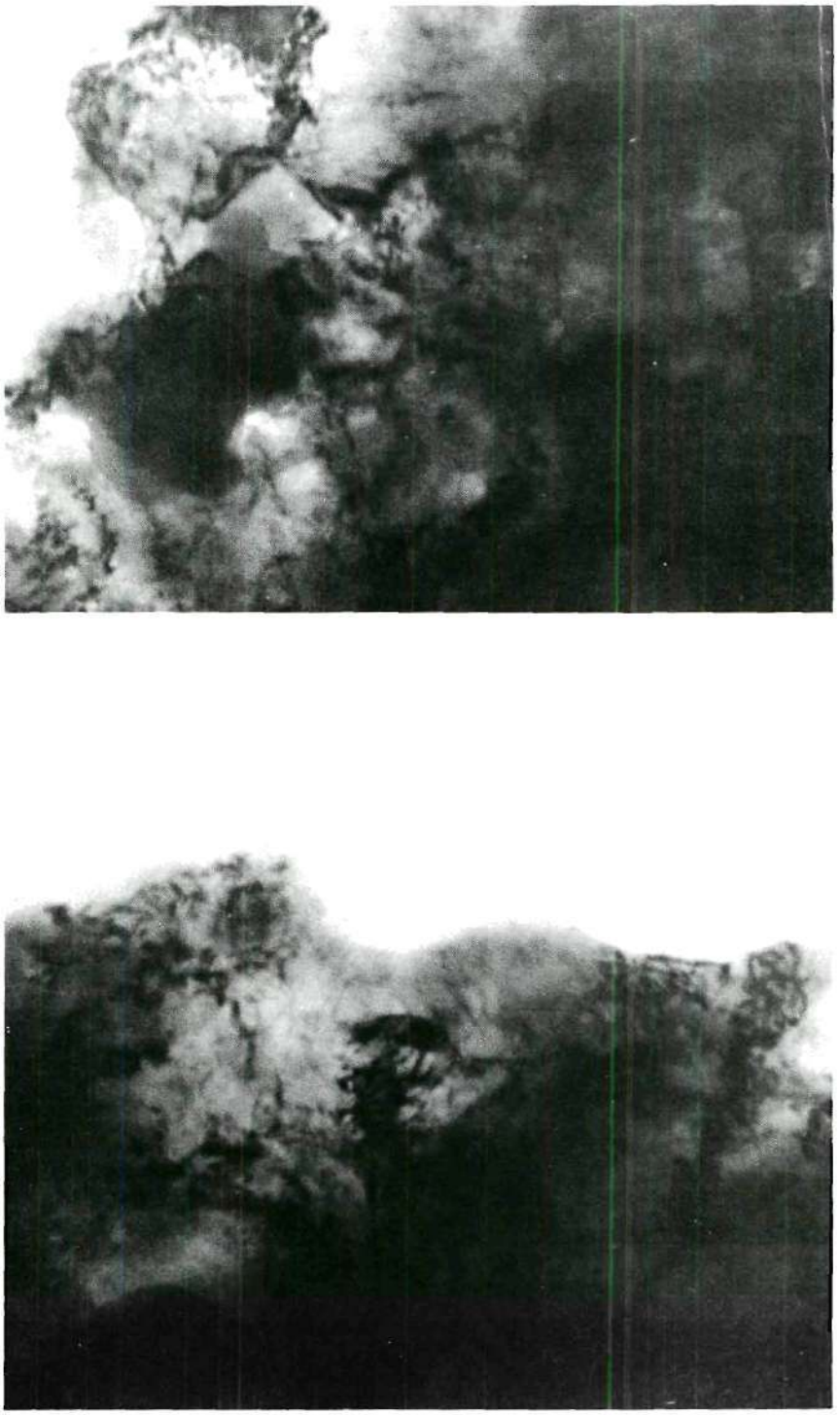

Figure 30. A Transmission Electron Micrograph of Almar 362. Specimen No. 1 Made Cathodic in a 50% HCl + 1% SeO_2 Solution.

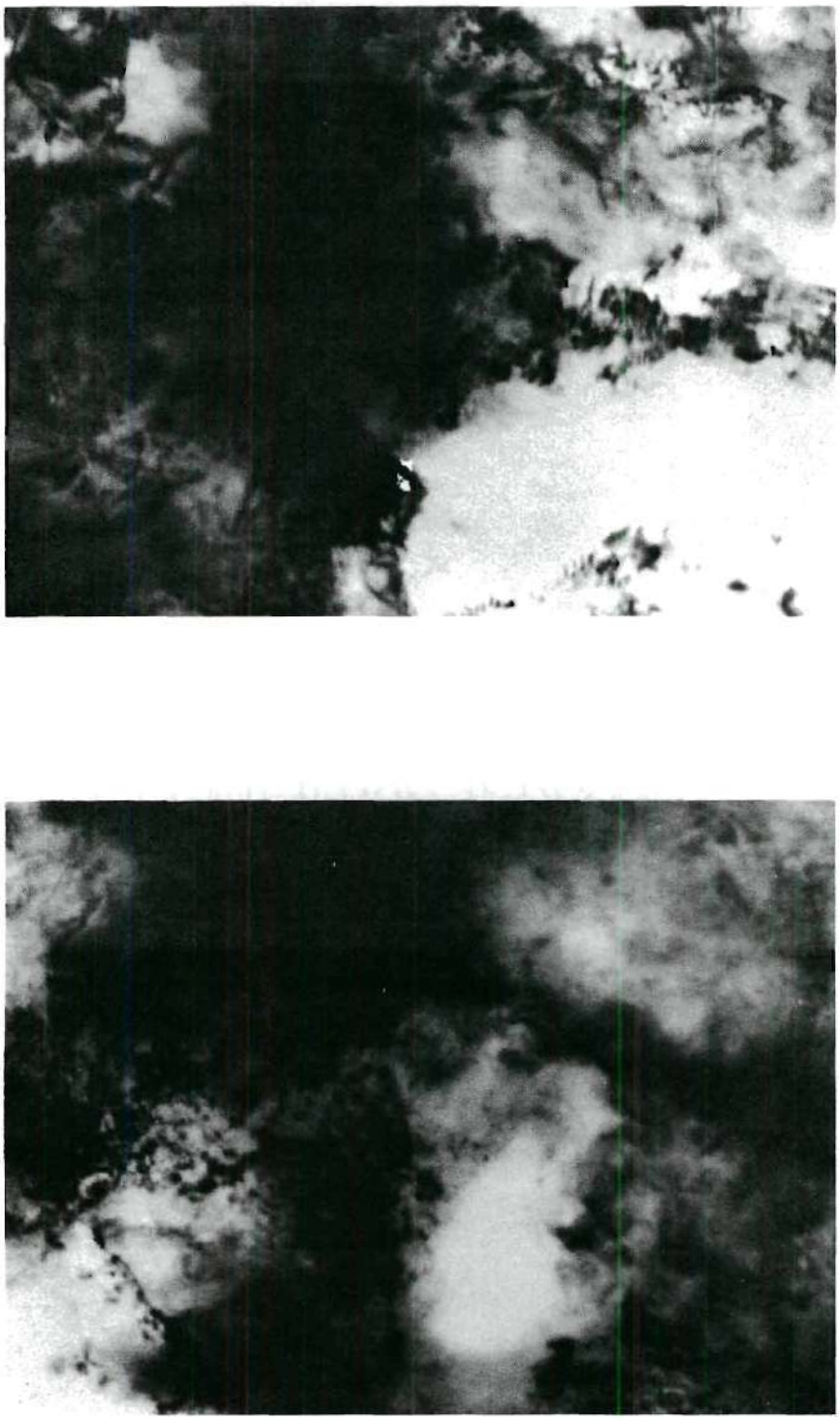

Figure 31. A Transmission Electron Micrograph of Almar 362. Specimen No. 1 Made Cathodic in a 12% NaCl Solution.

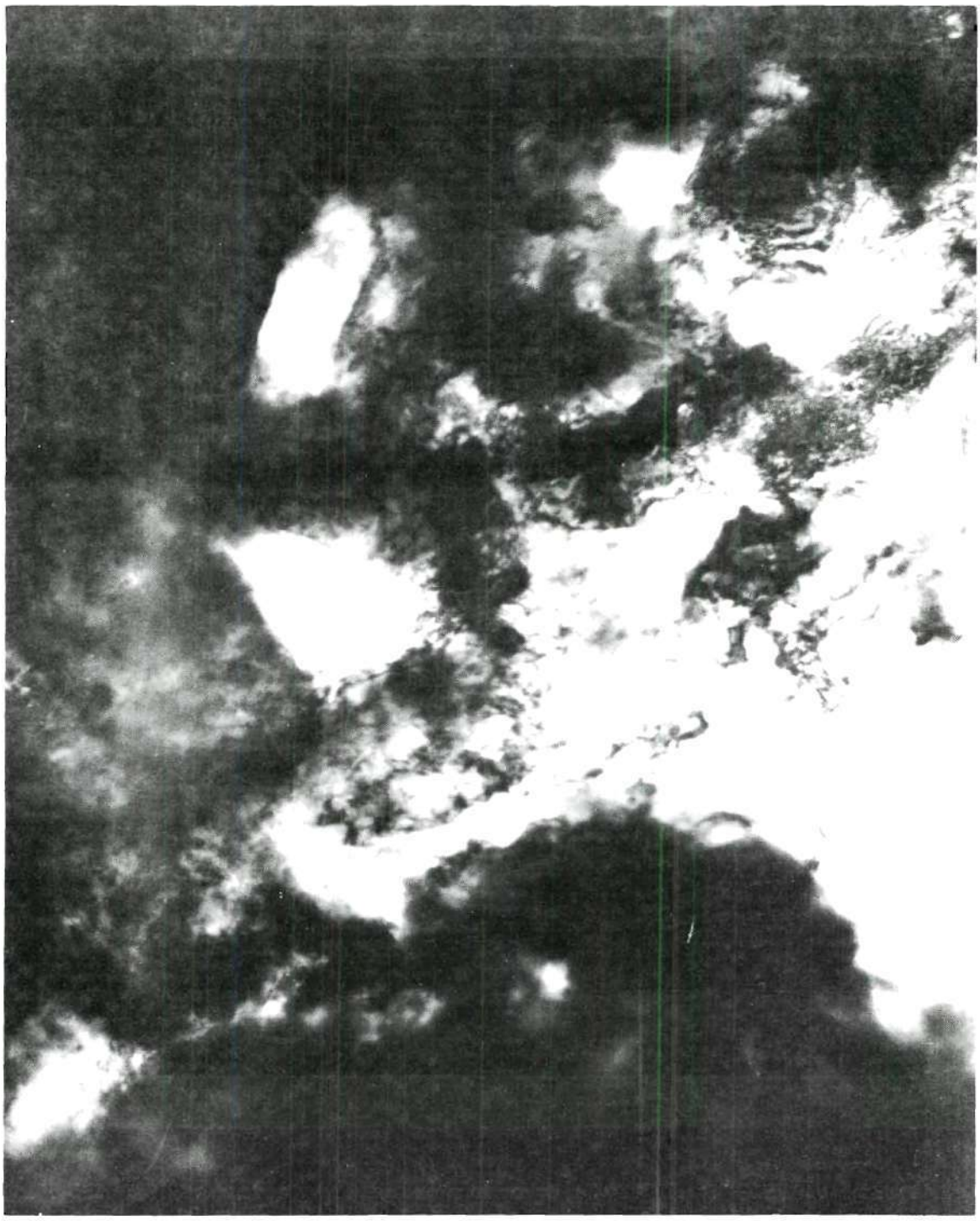

Figure 32. A Transmission Electron Micrograph of Almar 362. Specimen No. 2 Made Anodic in a 50% HCl + 1% SeO_2 Solution.

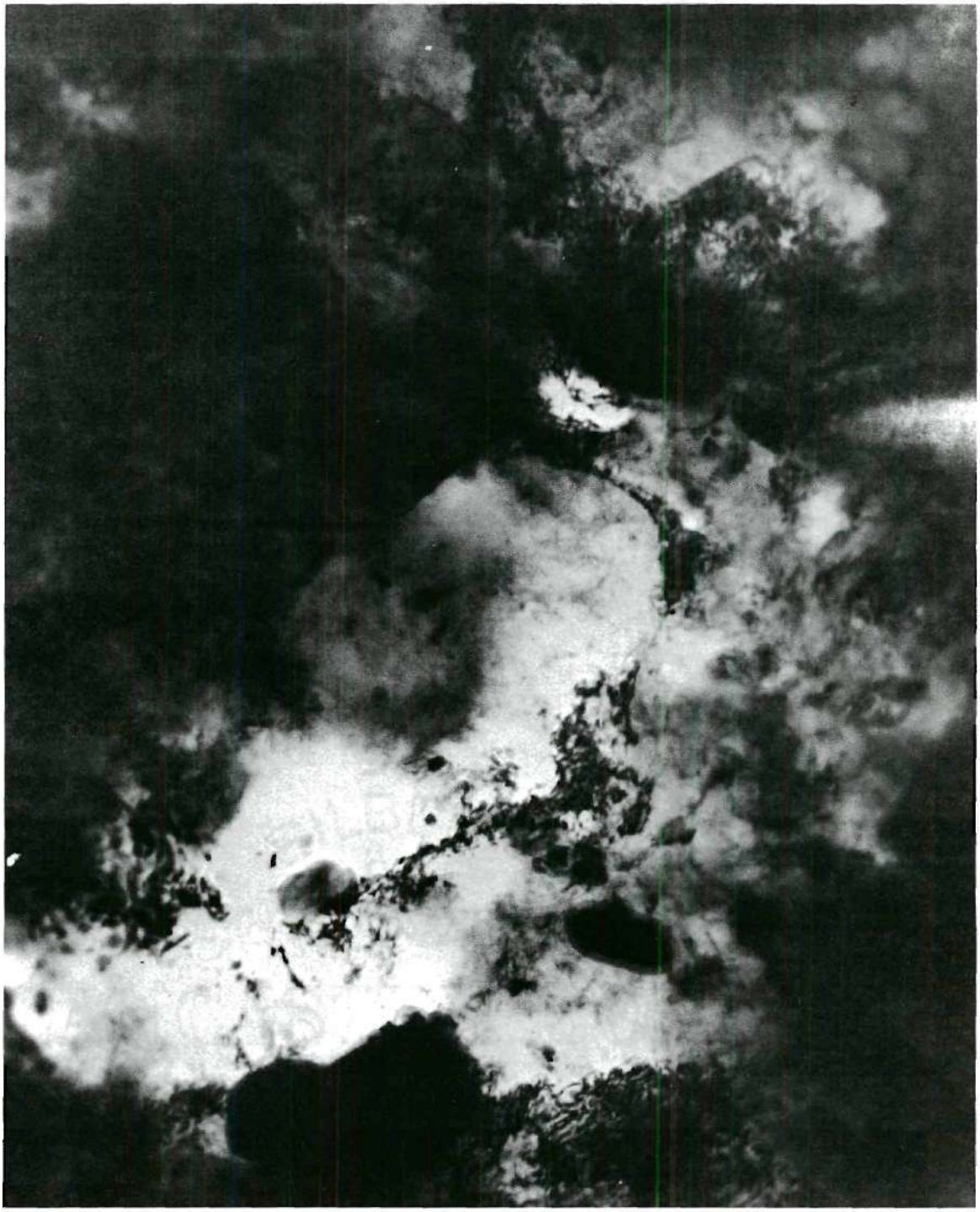

Figure 33. A Transmission Electron Micrograph of Almar 362. Specimen No. 2 Made Cathodic in a 50% HCl + 1% SeO_2 Solution.

to identify dislocations positively except when they lay almost in the plane of the foil. Many of the dot-like features in Figures 28 to 33 may be dislocation inclined to the plane of foil. Due to these difficulties, a crack formation theory based mainly on dislocation interactions would be impossible.

The general conclusion is that no differences between anodic and cathodic fractures of Almar 362 steel can be detected by transmission electron microscopy techniques.

CHAPTER V

CONCLUSIONS AND RECOMMENDATIONS

Conclusions

1. Almar 362 steel can be cracked by the right combination of heat treatment and environment; the susceptibility for cracking diminishes with decreasing strength of the material.
2. A significant fact is that this steel did not show susceptibility in NaCl solutions of any concentration unless additions of activating agents were made. This indicates Almar 362 is resistant to most chloride environments at the solution temperatures used.
3. The cracking behavior diminishes with decreasing applied stress, but no sign of a clear-cut minimum stress for cracking was found.
4. Almar 362 is more susceptible to cracking when cold-worked before aging.
5. Small positive impressed currents decrease the breaking time and small negative impressed currents on bent-beam specimens markedly increase the time to fracture.
6. Chloride solutions containing acetic acid or SeO_2 substantially decrease the notch strength of Almar 362.
7. No differences between anodic and cathodic fractures could be detected by metallographic and electron microscopy techniques; this indicates that the two processes may be fundamentally related.

Recommendation for Further Research

1. Work should be done at stresses well below yield strength since less susceptibility for cracking is obtained. This work would be useful for studying crack propagation.
2. The susceptibility to cracking should be studied for different degrees of cold work (cold rolling) for more thoroughly understanding the effect of cold work on the susceptibility for cracking.
3. The effects of aging time and temperature on cracking should be studied for over-aging and under-aging conditions.
4. More electron microscopy, metallography, and fractography studies on the two cracking processes, SCC and HEC, should be carried out as an aid in explaining the mechanism.

APPENDIX A

STRESS ANALYSIS OF BENT-BEAM STRESS CORROSION SPECIMENS

APPENDIX A

STRESS ANALYSIS OF BENT-BEAM STRESS CORROSION SPECIMENS

General Theory

Elastic stresses in bent-beam stress corrosion specimens were determined by mathematical large-deflection analysis (35). Relationships were established between maximum stress and specimen and holder dimensions, as well as between maximum deflection and these dimensions.

Stressing of a bent-beam specimen is a simple operation, shown schematically in Figure A-1. Ends of the specimen are forced toward each other so that their original distance L (length of unstressed specimen) is reduced to distance H of the loading jig support. Maximum stress in the specimen depends on unstressed length L, distance H, specimen thickness t, and specimen width b. From the stressing procedure shown in Figure A-1 it is seen that the specimen behaves as a buckled column; that is, it is subjected to an axial load of such magnitude that the deflected shape is an equilibrium configuration. Because deflections of the bent-beam specimen are quite large compared to the specimen thickness, the simplified small-deflection theory commonly used to solve column-buckling problems does not apply; therefore a large-deflection theory must be used.

Because the deflected shape of the specimen is an equilibrium configuration, the amount applied by the external force P at a cross

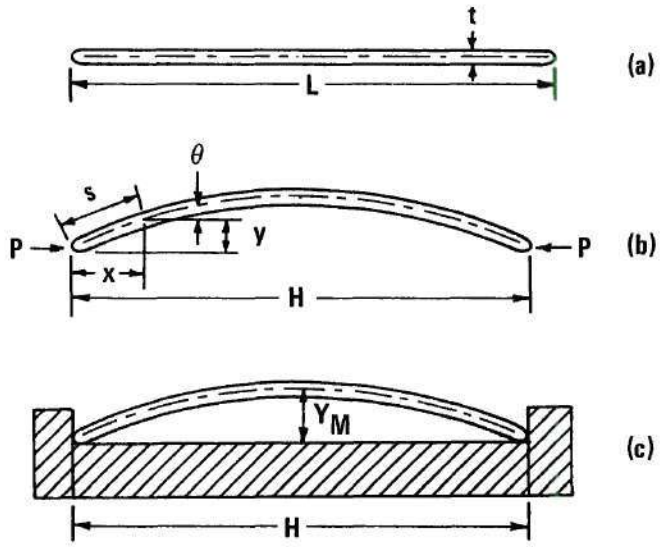

Figure A-1. Stressing of Bent-Beam Stress Corrosion Specimen.

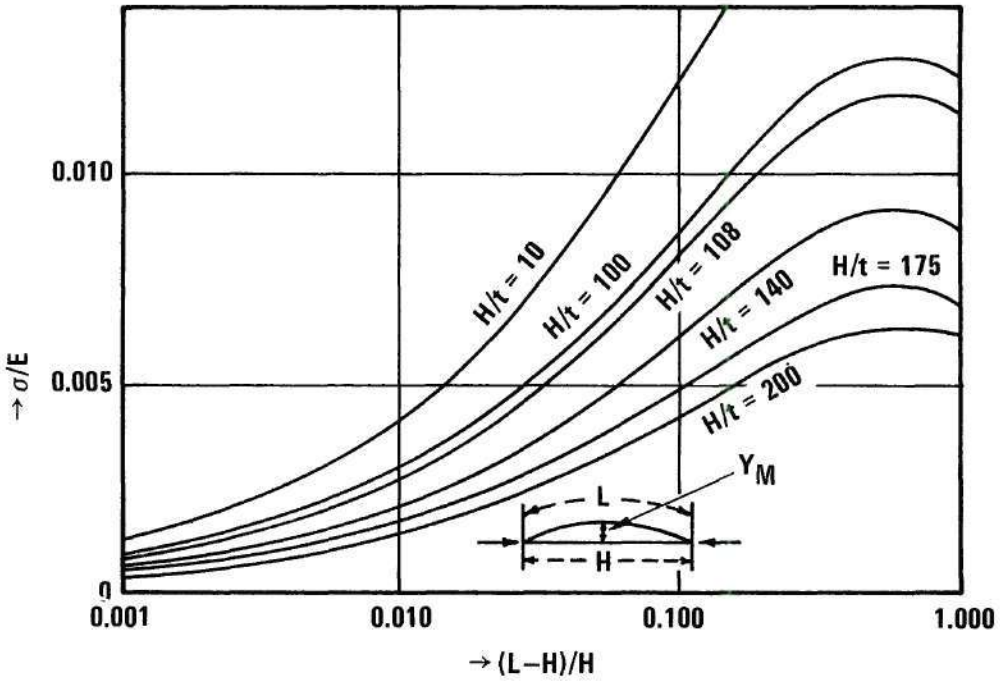

Figure A-2. Tensile Stress in Bent-Beam Stress Corrosion Specimen.

section of the specimen at any distance must be equal to the moment of the internal stresses present in that cross section. If the maximum stress in the specimen does not exceed the proportional limit of the material, the equilibrium condition gives the following differential equation:

$$M = PY = - E_m I \frac{d\theta}{ds} \tag{1}$$

In this equation P is the axial load, E_m is the modulus of elasticity of the material, I is the moment of inertia of the cross section ($I = \frac{1}{12} bt^3$ where b is the width and t is the thickness of the specimen), where as Y, θ, and s are defined as deflection, slope and arc length, respectively (Figure A-1 b).

As $dy/ds = \sin \theta$, differentiation of equation (1) with respect to s gives the following differential equation:

$$\frac{d^2\theta}{ds^2} + \lambda^2 \sin \theta = 0$$

$$\lambda^2 = \frac{P}{EmI} \tag{2}$$

Multiplication of equation (2) by $2\, d\theta/ds$ and integration of that expression gives:

$$\left(\frac{d\theta}{ds}\right)^2 = 2\lambda^2 \cos \theta - 2\lambda^2 \cos \theta_0$$

$$= 4\lambda^2[\sin^2(\theta_0/2) - \sin^2(\theta/2)] \tag{3}$$

where θ_0 is the maximum slope of the specimen (at x = 0).

Equation (3) can be solved by taking the square root of both sides, separating the variables and integrating. The result is as follows:

$$\int_{\theta_0}^{0} [\sin^2(\theta_0/2) - \sin^2(\theta/2)]^{-1/2} d\theta = \int_{0}^{L/2} - 2\lambda ds = - \lambda L \qquad (4)$$

The substitution $\sin(\theta/2) = k \sin u$ where $k = \sin(\theta_0/2)$ then gives

$$\frac{\lambda L}{2} = \int_{0}^{\pi/2} \frac{du}{\sqrt{1 - k^2 \sin^2 u}} \qquad (5)$$

The integration in equation (5) is known as the complete elliptic integral of the first kind and is denoted by K(k) so that equation (5) can be rewritten as

$$L = \frac{2K(k)}{\lambda} \qquad (6)$$

The maximum deflection Ym can be found from the integral

$$Ym = \int_{0}^{Ym} dy = \int_{0}^{L/2} \sin \theta \, ds \qquad (7)$$

It is found that

$$Ym = \frac{2K}{\lambda} \qquad (8)$$

The distance between the supports can be found from the integral

$$H = 2 \int_{0}^{H/2} dx = 2 \int_{0}^{L/2} \cos \theta \, ds \qquad (9)$$

or

$$H = \frac{4E(k) - 2K(k)}{\lambda} \tag{10}$$

In equation (10) E(k) denotes the integral

$$\int_0^{\pi/2} \sqrt{1 - K^2 \sin^2 u} \; du$$

which is known as complete elliptical integral of second kind. From equation (10) it is seen that

$$\lambda = \frac{4E(k) - 2K(k)}{H} \tag{11}$$

The magnitude of the applied force P is therefore

$$P = E_m I \lambda^2 = E_m I \left[\frac{4E(k) - 2K(k)}{H}\right]^2 \tag{12}$$

From equations (8), (11), (12) it follows that

$$M = PYm = 2E_m Ik \left[\frac{4E(k) - 2K(k)}{H}\right] \tag{13}$$

The maximum tensile stress σ is

$$\sigma = \frac{Mt}{2I} - \frac{P}{bt} \tag{14}$$

$$\sigma = 4E_m \left[2E(k) - K(k)\right]\left[\frac{k}{2} - \frac{2E(k) - K(k)}{12}\left(\frac{t}{H}\right)\right]\frac{t}{H} \tag{15}$$

By dividing both sides of the equation (15) by the modulus of elasticity E_m, we have the following expression for the maximum tensile strain:

$$\epsilon = \frac{\sigma}{E_m} = 4\left[2E'(k) - K'(k)\right]\left[\frac{k}{2} - \frac{2E(k) - K(k)}{12}\left(\frac{t}{H}\right)\right]\frac{t}{H} \qquad (16)$$

It is seen that ϵ is a function of parameter K. The relative difference between L and H is found from equations (6) and (10) to be as follows:

$$\frac{L - H}{H} = \frac{2[K(k) - E(k)]}{2E(k) - K(k)} \qquad (17)$$

Because $\frac{L - H}{H}$ is also a function of the parameter K, equation (16) and (17) establish the relationship between ϵ and $\frac{L - H}{H}$ in parameter form. This relationship is shown graphically in the Figure A-2 for H/t ratios ranging from 70 to 200. It is interesting to note that each curve has an upper limit which indicates that for each H/t a maximum strain exists that cannot be exceeded by increasing the relative difference between L and H.

Length Calculations (L) of Bent-Beam Specimens

Specimens Annealed, Cold Rolled, and Aged

Thickness = 0.05 inch

Specimen No. 1, aged 8 hours at $900^{\circ}F$

σ = 182,000 psi $\qquad$ $E = 29.5 \times 10^6$ psi

$\frac{\sigma}{E} = \frac{182,000}{29.5 \times 10^6} = 0.00618$ $\qquad$ $\frac{H}{t} = \frac{7.00}{0.05} = 140$

$\frac{L - H}{H} = 0.097$ $\qquad$ L = 7.674 inch

Specimen No. 2, aged 4 hours at $950^{\circ}F$

σ = 172,000 psi E = 29.5×10^6 psi

$\frac{\sigma}{E} = \frac{172,000}{29.5 \times 10^6} = 0.00583$

$\frac{L - H}{H} = 0.088$ L = 7.616 inch

Specimen No. 3, aged 3 hours at 1000°F

σ = 160,000 psi E = 29.5×10^6 psi

$\frac{\sigma}{E} = \frac{160,000}{29.5 \times 10^6} = 0.00542$

$\frac{L - H}{H} = 0.0700$ L = 7.495 inch

Specimen No. 4, aged 2 hours at 1050°F

σ = 144,000 psi E = 29.5×10^6 psi

$\frac{\sigma}{E} = \frac{144,000}{29.5 \times 10^6} = 0.0049$

$\frac{L - H}{H} = 0.056$ L = 7.393 inch

Specimen No. 5, aged 1 hour at 1150°F

σ = 115,000 psi E = 29.5×10^6 psi

$\frac{\sigma}{E} = \frac{115,000}{29.5 \times 10^6} = 0.00392$

$\frac{L - H}{H} = 0.033$ $\qquad$ $L = 7.231$ inch

Specimens Annealed and Aged

Thickness = 0.10 inch

Specimen No. 1, aged 8 hours at 900°F

$\sigma = 182{,}000$ psi $\qquad$ $E = 29.5 \times 10^6$ psi

$\frac{\sigma}{E} = \frac{182{,}000}{29.5 \times 10^6} = 0.00618$ $\qquad$ $\frac{H}{t} = \frac{7.00}{0.1} = 70$

$\frac{L - H}{H} = 0.022$ $\qquad$ $L = 7.154$ inch

Specimen No. 2, aged 4 hours at 950°F

$\sigma = 172{,}000$ psi $\qquad$ $E = 29.5 \times 10^6$ psi

$\frac{\sigma}{E} = \frac{172{,}000}{29.5 \times 10^6} = 0.00583$

$\frac{L - H}{H} = 0.0195$ $\qquad$ $L = 7.136$ inch

Specimen No. 3, aged 3 hours at 1000°F

$\sigma = 160{,}000$ psi $\qquad$ $E = 29.5 \times 10^6$ psi

$\frac{\sigma}{E} = \frac{160{,}000}{29.5 \times 10^6} = 0.00542$

$\frac{L - H}{H} = 0.018$ $\qquad$ $L = 7.126$ inch

APPENDIX B

NOTCH STRENGTH CALCULATIONS

APPENDIX B

NOTCH STRENGTH CALCULATIONS

Material Annealed and Aged

Typical Test without Corrodent

$w = 1"$ (see Figure 7)

$B = 0.1"$

$\alpha_0 = 0.15"$

$B(W - 2\alpha_0)$ values:

No. 1 $0.101(1.006-0.3) = 0.0706$ in.^{2}

No. 2 $0.100(1.005-0.3) = 0.0705$ in.^{2}

No. 3 $0.100(1.005-0.3) = 0.0705$ in.^{2}

No. 4 $0.101(1.003-0.3) = 0.0703$ in.^{2}

No. 5 $0.100(1.002-0.3) = 0.0702$ in.^{2}

ultimate load (P):

No. 1 15625 lbs.

No. 2 15450 lbs.

No. 3 15350 lbs.

No. 4 15150 lbs.

No. 5 13050 lbs.

$\sigma_{NS} = \frac{P}{B(W - 2\alpha_0)}$:

No. 1 222,000 psi

No. 2 220,000 psi

No. 3 217,000 psi

No. 4 215,000 psi

No. 5 186,000 psi

Test with Corrodent 10% NaCl + 5% HA_c

$B(W - 2\alpha_0)$ values:

No. 1 $0.1(1.006-0.3) = 0.0706$ in.^{2}

No. 2 $0.1(1.013-0.3) = 0.0713$ in.^{2}

No. 3 $0.1(1.010-0.3) = 0.0710$ in.^{2}

No. 4 $0.1(1.008-0.3) = 0.0708$ in.^{2}

No. 5 $0.1(1.025-0.3) = 0.0725$ in.^{2}

ultimate load (P):

No. 1 14,360 lbs.

No. 2 15,300 lbs.

No. 3 14,800 lbs.

No. 4 14,750 lbs.

No. 5 13,000 lbs.

$\sigma_{NS} = \frac{P}{B(W - 2\alpha_0)}$:

No. 1 203,000 psi

No. 2 214,500 psi

No. 3 208,000 psi

No. 4 203,000 psi

No. 5 172,000 psi

Material Annealed, Rolled, and Aged

Test with Corrodent 10% NaCl + 5% HA_c at Room Temperature

$B(W - 2\alpha_0)$ values:

No. 1 $0.05(0.958-0.3) = 0.03290$ in.^{2}

No. 2 $0.05(0.955-0.3) = 0.03275$ in.^{2}

No. 3 $0.05(0.949-0.3) = 0.03245$ in.^{2}

No. 4 $0.05(0.948-0.3) = 0.03290$ in.^{2}

No. 5 $0.05(0.947-0.3) = 0.03239$ in.^{2}

ultimate load (P):

No. 1	5,600 lbs.
No. 2	5,500 lbs.
No. 3	5,500 lbs.
No. 4	5,800 lbs.
No. 5	5,550 lbs.

$\sigma_{NS} = \frac{P}{B(W - 2\alpha_0)}$:

No. 1	170,000 psi
No. 2	168,000 psi
No. 3	168,000 psi
No. 4	166,000 psi
No. 5	171,000 psi

Test with Corrodent 10% NaCl + 5% HA_c at 70°C

$B(W - 2\alpha_0)$ values:

No. 1 $0.05(0.960-0.3) = 0.0330$ in.^{2}

No. 2 $0.05(0.960-0.3) = 0.0330$ in.^{2}

No. 3 $0.05(0.955-0.3) = 0.3275$ in.^{2}

No. 4 $0.05(0.960-0.3) = 0.0330$ in.^{2}

No. 5 $0.05(0.953-0.3) = 0.03265$ in.^{2}

ultimate load (P):

No. 1	4,700 lbs.
No. 2	4,800 lbs.
No. 3	4,700 lbs.
No. 4	4,500 lbs.
No. 5	4,900 lbs.

$\sigma_{NS} = \frac{P}{B(W - 2\alpha_o)}$:

No. 1	142,000 psi
No. 2	146,000 psi
No. 3	142,000 psi
No. 4	136,000 psi
No. 5	150,000 psi

BIBLIOGRAPHY

1. Fraser, J. P. and R. S. Treseder, "Cracking of High Strength Steels in Hydrogen Sulfide Solutions," Corrosion 8: 342-350, October (1952).

2. Bloom, F. K., "Stress Corrosion Cracking of Hardenable Stainless Steels," Corrosion 11: 351t-361t, (1955).

3. Fontana, M. G., "Stress Corrosion Cracking in Type 403 Stainless Steel," WADC Tech. Report, 56-242 (1956) 51 pp.

4. Naumann, F. K. and W. Carins, "The Importance of the Corrosion Processes in Aqueous Hydrogen Sulfide Solution for the Formation of Fracture in Steels," Arch. Eisenhuttenu 30: 283-292 (1959).

5. Trozzo, P. S. and R. F. McCartney, "Relationship of Microstructure and Stress Corrosion Cracking of Type 410 Stainless Steel," Corrosion 16: 26-30, March (1960).

6. Phelps, E. H. and R. B. Mears, "The Effect of Composition and Structure of Stainless Steel Upon Resistance to Stress-Corrosion Cracking," First International Congress on Metallic Corrosion, London: Butterworths, pp. 319-327 (1962).

7. Slunder, G. J. and W. Boyd, "Environmental and Metallurgical Factors of Stress Corrosion Cracking in High Strength Steels," Battelle Memorial Institute DMIC Report 151 (1961) 21 pp.

8. Durkin, A. E., "Corrosion Cracking of Martensitic Stainless Steel," Metal Progress 64: 72-75 (1953).

9. Johnson, H. E., "Laboratory Evaluation of High Strength Steels," Cornell University NRL Tech Memo 17, October (1961).

10. Robinson, R. B. and R. J. Uzdarwin, "Investigation on Stress-Corrosion Cracking of High-Strength Alloys," Aerojet General Corporation, Annual Summary Report No. 2092 (1961).

11. Slunter, G. J., "Stress Corrosion Cracking of High-Strength Stainless Steels in Atmospheric Environments," Battelle Memorial DMIC Report 158 (1961) 38 pp.

12. Jackson, R. P., "Stress Corrosion Cracking of 17-4 PH Stainless Steel," E. I. DuPont de Nemours and Co., Savannah River Laboratory, Report P-779 (1962) 7 pp.

13. Owen, C. J., "Stress Corrosion of High Strength Steels and Alloys," Mellon Institute, Final Report (Contract No. DA-36-034-ORD-3277RD) (1962), 110 pp.

14. Weibull, I., "Stress Corrosion Cracking in High Strength Steel- or Hydrogen Embrittlement," Advances in Aeronautical Sciences, Pergamon Press 3: 335-356 (1962).

15. Setterlund, R. B., "Investigation of Stress-Corrosion Cracking of High-Strength Alloys," General Corporation Report L0414-01-22, May (1963), 4 pp.

16. Decker, R. F., J. T. Eash and A. J. Goldman, "18% Nickel Mar-aging Steel," Transactions of the ASM Volume 55, 59-77 (1962).

17. Lillys, P. and A. E. Nehrenberg, "Effect of Tempering Temperature on Stress-Corrosion Cracking and Hydrogen Embrittlement of Martensitic Stainless Steel," Trans. AMS 48: 327-355 (1956).

18. Bhatt, H. J. and E. Phelps, "Effect of Solution PH on the Mechanism of Stress Corrosion Cracking of a Martensitic Stainless Steel," Corrosion 17: 430t-434t (1961).

19. Brown, B. F., "Stress Corrosion Cracking and Related Phenomena in High-Strength Steels," Naval Research Laboratory, May (1966).

20. Johnson, H. H., "Calibration of the Electrical Resistance Method of Studying Crack Propagation," Cornell University, NRL Tech. 205 (Contract Nonr-3286(01)) May (1962), 10 pp.

21. "Almar 362 a Mar-aging Stainless Steel," Published by the Allegheny Ludlum Steel Corporation.

22. Lacques, Friedel, "Dislocations."

23. Scharfstein, L. R. and E. Eisenbrown, "Potential-time Curves Obtained During the Stress Cracking of Metals," Nature 188: 572-573 (1960).

24. Suss, H., "Shot Peening of Metals for Protection Against Stress Corrosion Cracking," Corrosion 18: 17t-20t (1962).

25. (Anonymous), "Oil Well Materials for Resistance to Hydrogen Sulfide or Stress Corrosion Cracking," Materials Protection 2(3): 93-94, March (1963).

26. Uhlig, H. H., "Action of Corrosion and Stress on 13% Cr Stainless Steel," Metal Progress 57: 486-487 (1950).

27. Irwin, G. R. and S. E. Srawley, "Progress in the Development of Crack Toughness Fracture Tests," ASTM Bull. No. 1, 1-11, January (1962).

28. Brown, B. F., "Notch Sensitivity Effects in Stress Corrosion and Hydrogen Embrittlement Tests on High Strength Steels," Corrosion 15: 399t-402t (1959).

29. Davis, R. A., "Stress Corrosion Cracking Investigation of Two Low Alloy High Strength Steels," Corrosion 19: 45t-55t (1963).

30. Johnson, H. H., "Preliminary Comments on the Role of Water Vapor in Slow Crack Growth in High Strength Steels," Cornell University, NRL Tech. 208, April (1962), 3 pp.

31. Badger, W. L., "Stress Corrosion of 12% Cr Stainless Steel," Trans. SAE 62: 307-313 (1954).

32. Halbig, J. and O. Ellis, "Observations on Corrosion Resistance of High Strength Stainless Steel for Aircraft," Corrosion 14: 389t-395t (1958).

33. Srawley, J. E., "Hydrogen Embrittlement Susceptibility of Some Steel," NRL Report 5392, October (1959), 25 pp.

34. Phelps, E. H. and A. W. Loginow, "Stress Corrosion of Steel for Aircraft and Missiles," Corrosion 10, 95-98, April (1964).

35. Haaijer, G. and A. W. Loginow, "Stress Analysis of Bent-Beam Corrosion Specimens," National Association of Corrosion Engineers 21: 105-111, April (1965).

36. Phelps, E. J. and A. W. Loginow, "Stress Corrosion of Steel for Aircraft and Missiles," Corrosion 16: 325t-335t (1960).